



ISSN : 2800-1729

Edition : Vol 1. Num 2 (2022)

# Biopolymer Applications Journal



Editor in chief:

**Pr. HAMMICHE Dalila**



UNIVERSITÉ ABDERRAHMANE MIRA - BEJAIA  
FACULTÉ DE TECHNOLOGIE



## **Biopolymer Applications Journal**

### **Editorial**

Biopolymer Applications Journal is a specialized scientific journal, created in 2021 and published by the *Faculty of Technology, University of Bejaia*. It appears twice a year and fills the need for researchers and engineering in biopolymers field. The journal is a space for inspiring ideas and discussions of advances in the field of biopolymer applications in a wide range of disciplines for the publication of high-quality peer-reviewed original papers and review articles.

The journal is interdisciplinary in regard to contributions and covers the following subjects:

-Ageing; Biochemistry;  
Bioengineering; biomaterials,  
biomedical engineering;  
mechanical engineering; modeling  
and simulation; polymers and  
plastics and other related topics.

### **Journal Information**

Biopolymer Applications Journal is a new Journal, where we aim to work towards spreading awareness about various disciplines amongst people from all walks of life through publication of articles with this Journal. We are offering you open Access, Peer-Reviewed, Rapid, and free Publication

**e-ISSN** 2800-1729

**Site web:** <http://www.univ-bejaia.dz/baj/>

**Contact:** [baj.contact@yahoo.com](mailto:baj.contact@yahoo.com)

**online submission:** <http://univ-bejaia.dz/revueBaj>

### **Editor-in-Chief**

Pr. Dalila HAMMICHE  
Université de Bejaia, Algeria  
[Baj.contact@yahoo.com](mailto:Baj.contact@yahoo.com)  
[Dalila.hammiche@univ-bejaia.dz](mailto:Dalila.hammiche@univ-bejaia.dz)

### **Editorial Board:**

Pr. Balbir Singh KAITH  
[kaithbs@nitj.ac.in](mailto:kaithbs@nitj.ac.in)  
NIT Jalandhar, Dr BR Ambedkar  
National Institute of Technology,  
Jalandhar, Punjab India

Pr. Amar BOUKERROU  
[amar.boukerrou@univ-bejaia.dz](mailto:amar.boukerrou@univ-bejaia.dz)  
Université Abderrahmane Mira de  
Béjaia

Dr. Vikram PANDIT  
[vikramupandit@hvdesaicollege.org](mailto:vikramupandit@hvdesaicollege.org)  
The Poona Gujarati Kelwani  
Mandal's, Haribhai V. Desai College,  
India

Dr. Abdelhakim BENSLIMANE  
[abdelhakim.benslimane@univ-bejaia.dz](mailto:abdelhakim.benslimane@univ-bejaia.dz)  
Université Abderrahmane Mira de  
Béjaia

Dr. Sofiane FATMI  
[sofiane.fatmi@univ-bejaia.dz](mailto:sofiane.fatmi@univ-bejaia.dz)  
Université Abderrahmane Mira de  
Béjaia

Dr. Chadia BENMERAD  
[chadia.benmerad@univ-bejaia.dz](mailto:chadia.benmerad@univ-bejaia.dz)  
Université Abderrahmane Mira de  
Béjaia

Pr. Denis RODRIGUE  
[denis.rodrigue@gch.ulaval.ca](mailto:denis.rodrigue@gch.ulaval.ca)  
Université Laval, Canada

Pr. Jean-François GERARD  
[jean-francois.gerard@insa-lyon.fr](mailto:jean-francois.gerard@insa-lyon.fr)  
INSA de Lyon, France

Pr. Mostapha TARFAOUI  
[mostapha.tarfaoui@ensta-bretagne.fr](mailto:mostapha.tarfaoui@ensta-bretagne.fr)  
Université de Bretagne Nord, France

Pr. Jannick DUCHET  
[jannick.duchet@insa-lyon.fr](mailto:jannick.duchet@insa-lyon.fr)  
INSA de Lyon, France

Dr. Ghozlène MEKHOLOUFI  
[ghozlene.mekhloufi@universite-paris-saclay.fr](mailto:ghozlene.mekhloufi@universite-paris-saclay.fr)  
Université de Paris Saclay, France

Carlos Manuel Silva  
[carlos.manuel@ua.pt](mailto:carlos.manuel@ua.pt)  
Université d'Aveiro, Portugal

Dr. Noamen GUERMAZI  
[noamen.guermazi@enis.tn](mailto:noamen.guermazi@enis.tn)  
Université de Sfax, Tunisie

Dr. Alain BOURMAUD  
[alain.bourmaud@univ-ubs.fr](mailto:alain.bourmaud@univ-ubs.fr)  
Université de Bretagne Sud, France

Dr. Ahmed ABDULRAZZAQ  
[aarhrf@mu.edu.iq](mailto:aarhrf@mu.edu.iq)  
Al-Muthanna University, Iraq

Dr. Neethu NINAN  
[neethun.ninan@gmail.com](mailto:neethun.ninan@gmail.com)  
University of South Australia,  
Australia

Dr. Shivaji PANDIT  
[drsspandit65@gmail.com](mailto:drsspandit65@gmail.com)  
Satral College Pravaranagar, India

Dr. Adel BENIDIR  
Centre National d'Etudes et de  
Recherches intégrées du Bâtiment  
(CNERIB)  
[benidir.adel@yahoo.fr](mailto:benidir.adel@yahoo.fr)

Dr. Mohamed Amine  
KHADIMALLAH  
[mohamedamine.khadimallah@fsgf.ru.u.tn](mailto:mohamedamine.khadimallah@fsgf.ru.u.tn)  
Prince Sattam Bin Abdulaziz  
University, College of Engineering,  
Alkharij, Saudi Arabia  
University of Carthage, Polytechnic  
School of Tunisia, Laboratory of  
Systems and Applied Mechanics,  
Tunisia

Pr. Rabah FERHOUM  
[ferhoum@yahoo.fr](mailto:ferhoum@yahoo.fr)  
Université de Tiziouzeu

Pr. Mansour ROKBI  
mansour.rokbi@univ-msila.dz  
Université de M'sila, Algeria

Dr. Ali DEBIH  
ali.debih@univ-msila.dz  
Université de M'sila, Algeria

Pr. Lakhdar SEDIRA  
sedira.lakhdar@gmail.com  
Université de Biskra, Algeria

Dr. Rakesh Kumar  
[rakeshkumar@nitj.ac.in](mailto:rakeshkumar@nitj.ac.in)  
NIT Jalandhar, Dr BR Ambedkar  
National Institute of Technology,  
Jalandhar, Punjab, India

## Table of content

*Rebiha BELLACHE, Dalila HAMMICHE, Amar BOUKERROU*

Elaboration of ointments based on vegetable plants “*Calendula arvensis*” and “*Dandelion*”. Vol 1, N° 2, 2022, pp.01-07

*Aicha DEHANE, Dalila HAMMICHE, Amar BOUKERROU, Balbir Singh KAITH*

An investigation of the mechanical properties of starch biofilms plasticized by glycerol. Vol 1, N° 2, 2022, pp. 08-13

*Nadira BELLILI, Badrina DAIR, Noura HAMOUR, Hocine DJIDJELLI, Amar BOUKERROU*

Perfection of a composite material reinforced by a natural filler modified by a gamma irradiation treatment. Vol 1, N° 2, 2022, pp. 14-18

*Ganesh Kavita Parshuram JADHAV, Omkar Sadhna Arun MALUSARE, Ragini Kundan Prashant*

*AHIWALE, Purnima PATIL, Ayoub GROULI, Mohammed BERRADA, Vikram Rama Uttam PANDIT*  
Safranin dye degradation by using Fe<sub>2</sub>O<sub>3</sub>-SnO<sub>2</sub> Nanocomposites under natural Sunlight. Vol 1, N° 2, 2022, pp.19-23

*Lamia TAOUZINET, Sofiane FATMI, Malika LAHIANI-SKIBA, Mohamed SKIBA, Mokrane IGUER-OUADA*

Nano-Encapsulation Systems Improve Drug Delivery and Solubility. Vol 1, N° 2, 2022, pp. 24-30

*Lisa KLAAI, Sonia IMZI, Dalila HAMMICHE, Amar BOUKERROU*

Preparation and Characterization of Starch Based Bioplastic Film from Potatoes. Vol 1, N° 2, 2022, pp.31-33

*Badrina DAIRI, Nadira BELLILI, Hocine DJIDJELLI, Amar BOUKERROU*

Evaluation of mechanical and water absorption properties of polypropylene/recycled poly (ethylene terephthalate) blends. Vol 1, N°2, 2022, pp.34-39

# Elaboration of ointments based on vegetable plants “*Calendula arvensis*” and “*Dandelion*”.

Rebiha BELLACHE\*, Dalila HAMMICHE, Amar BOUKERROU

Laboratoire des Matériaux Polymères Avancés, Département Génie des Procédés, Faculté de Technologie, Université de Bejaia, Algérie.

Corresponding author email\* [rebiha.bellache@univ-bejaia.dz](mailto:rebiha.bellache@univ-bejaia.dz)

Received: 10 May 2022; Accepted: 10 June; Published: 21 July 2022

---

## Abstract

*The synthetic chemical ointments produced by the cosmetic and pharmaceutical industries cause irritations and skin diseases. For this reason, the present work aims to prepare ointments based on two vegetable plants belonging to the same genus but with two different families, Calendula arvensis CA and Dandelion D, according to a protocol of variation of ratios between the beeswax and the infused oil of each flower of the two plants. Physico-chemical analyses are carried out to see the macroscopic and microscopic aspect, the resistance to water and pH as well as the conductivity, and the chemical structure of the ointments.*

*According to the obtained results, the Ratio R (1/3) of the CA ointment presents a better homogeneity, a better pH, Conductivity and a better physical stability by its water resistance, in addition to a better chemical stability by the increase at the level of all its characteristic bands.*

**Keywords:** ointment, *Calendula arvensis*, *Dandelion*, physico-chemical properties.

---

## I. Introduction

The pharmacological treatment of disease began long ago with the use of herbs [1]. By definition, ‘traditional’ use of herbal medicines implies substantial historical use, and this is certainly true for many products that are available as ‘traditional herbal medicines’ [2].

Our choice fell on *calendula arvensis* (CA) with yellow flowers and *Dandelion* (D) with orange flowers (Figure 1), which are renowned medicinal plants, used for a long time for their anti-inflammatory, soothing and healing properties, especially in dermatology.

Several *Calendula* preparations are available for incorporation in topical formulations directed towards wound healing and for soothing inflamed and damaged skin, like extracts, tinctures, and oils [3]. *Calendula* flower extract is the most frequently used in cosmetic products [4]. This plant contains several bioactive compounds, including terpenoids and terpenes (mainly bisabolol, faradiol, chamazulene, arnidiol and esters), carotenoids (mainly with rubixanthin and lycopene structures), flavonoids, (mainly quercetin, isorhamnetin and kaempferol aglycones) and polyunsaturated fatty acids, (mainly calendic acid) [5].

*Dandelion* (*Taraxacum officinale*) has been used in folklore medicine and traditional Chinese medicine in the treatment of inflammation and several women’s diseases such as breast and uterine cancers [6], and it is also acclaimed as a nontoxic medicinal herb with exceptional values for its choleric, anti-rheumatic [7], diuretic [8], and anti-inflammatory properties [9]. Several flavonoids including caffeic acid, chlorogenic acid, luteolin, and luteolin 7- glucoside have been isolated from the *Dandelion* [10]. This latter is a rich source of vitamins A, B complex, C, and D, as well as minerals such as iron, potassium, and zinc [11].

Today, many products essentially cosmetic and pharmaceutical [12] contain *calendula arvensis* and even *Dandelion*, like ointments and creams, and avoid chemical synthesis products that cause irritation and skin diseases.

The main objective of this study is to prepare ointments based on two plants of the same genus and different family, *Calendula arvensis* and *Dandelion*. For this purpose, different physico-chemical characterizations were carried out for these preparations.



Figure 1: *Calendula arvensis* (CA) and *Dandelion* (D)

## II. Materials and Methods

### II.1. Materials

Whole plants of *Calendula arvensis* and *Dandelion* were collected from the campus of university of Bejaia-Algeria. Beeswax is one of the natural raw materials used in this study. As well as olive oil obtained by hot extraction.

### II.2. Methods

Dry two handfuls of *calendula arvensis* or *Dandelion* flowers in an oven set at a temperature of 45°C for four days (04), and then let them infuse in 250 ml of olive oil for about three weeks (03). Then melt the wax over low heat in a crystallizer to about 60 to 70°C and add the infused oil to it and simmer for about 10 to 15 minutes until you have a homogeneous oily solution. After the cooling of this latter,

an ointment will be formed with a consistency that differs from the different ratios R (beeswax/olive oil) prepared (R1/1, R1/2 and R1/3).

### III. Characterizations

- **The pH measurements and conductivities.**
- **Morphological aspect and water resistance:** in order to observe the macroscopic surface and its homogeneity microscopically, in addition to the water resistance when we have deposited a droplet of water on thin layer of ointment, the photos were taken of the different samples using an optical microscopy.
- **Chemical analysis:** FTIR spectra of the different samples were recorded using Agilent Technologies Cary 630 FTIR in the range of 4000-400 cm<sup>-1</sup> with a resolution of 4 cm<sup>-1</sup>.

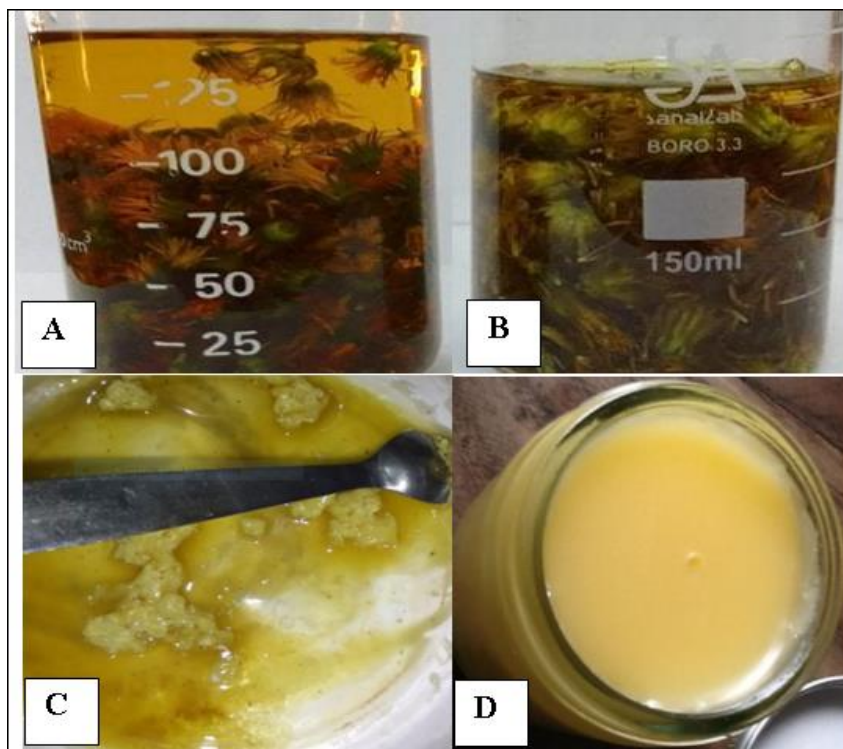


Figure 2: A- infused oil of *calendula arvensis*, B- infused oil of *Dandelion*, C- Beeswax, D- Ointment prepared

#### IV. Results and discussion

##### IV.1. Measurement of pH and conductivity

According to the Table 1 of the pH of the oils, we notice that the pH of the oil infused CA is more acid than that of oil infused D. Concerning the ointments, the pH of the yellow flowers DO one is more acid than the orange flowers

CAO. This led to an increase in conductivity, which can be explained by the displacement of ions.

In conclusion, the orange flower ointments CAO have better pH values than 5.25, which explains why our ointments are usable, and therefore we can carry out other characterization analyses.

**Table 1:** Measurement of pH and conductivity of different ointments

Samples	pH	Conductivity(μs/cm)
Olive oil	6.82	2.80
Infused oil CA	5.44	3.00
Infused oil D	5.23	3.32
R(1/1) CAO	5.25	2.80
R(1/2) CAO	5.46	3.00
R(1/3) CAO	5.80	2.60
R(1/1) CD	5.17	2.20
R(1/2) CD	5.24	3.00
R(1/3) CD	5.33	2.70

##### IV.2. Macroscopic aspect

All the ointments of different ratios (see Table 2), present a homogeneity before and after the application on the skin as well as they present a yellowish color for DO and an orangeade for CAO.

But a different consistency (fluid for the R (1/1), less consistent for the R (1/2), and more consistent like a vaseline for the R (1/3)).

Therefore, the preparation method allowed obtaining a very good homogeneity for all ointments prepared.

**Table 2:** Macroscopic aspect of DO and CAO (Before and after application on the skin)







Ratio	DO (Before and after application on the skin)	CAO (Before and after application on the skin)
R 1/1		
R 1/2		
R 1/3		



Figure 3: Microscopic aspect of CAO and DO

### IV.3. Microscopic aspect

According to the Figure 3 prepared ointments have a better physical stability; the latter is characterized by a homogeneous appearance, which was found for all prepared ointments of CA and D.

### IV.4. Water resistance

All the prepared ointments are non-miscible, non-adherent to skin and have an almost spherical shape,

especially for the ratio (1/3). As a result, all the ointments are resistant for water, especially for this latter ratio.

Generally speaking, water and wax are an hydrophobic aspect; they form a barrier on the surface of the skin, limit the evaporation of the water contained in the skin and thus increase its hydration. Consequently, these ointments are hydrophobic ointments, which do not dry out and remain on the surface of the skin for a long time and do not wash off with water.

Table 3: Water resistance of CAO and DO

Ratio	CAO	DO
R 1/1		
R 1/2		
R 1/3		

### IV.5. Chemical analysis

Figure 4 shows the infrared spectrum of the infused oils and olive oil. From obtained results by chemical analysis, it is noted that all the spectra have the same appearance {virgin before and after infusion}. However, an increase in the intensities of the peaks for the infused oils compared to the virgin oil (which are listed in Table 3 [13]) especially for the orange flowers CA, as well as a finding of an increase in transmittance for the yellow flowers D, which is due to its transparency compared to the orange flowers CA.

This principle can be explained by an addition of the characteristic bands contained in the orange and yellow

plants to those already existing in the virgin oil. Concerning the comparison between the spectra of the orange flower ointments CAO (Figure 5), the R (1/3) shows an increase in intensity in all the bands, which corresponds to the best chemical stability, and its results have been confirmed by the visual, microscopic and water resistance analysis.

To this effect, there is a proportional relationship between the amount of oil and the physic-chemical stability.

The same remarks and interpretations for the yellow flower ointments DO (Figure 6) have been drawn.



Table 4: FTIR of olive oil [12]

Bands (cm <sup>-1</sup> )	Fonctionnel groups
3005.64	O-H
2925.71	O-H
2855.17	C-H
1746.39	C=O
1462.38	C=C
1373.98	O-H
1231.97	C-O-
1161.44	C-O-
720.01	-CH <sub>2</sub> -

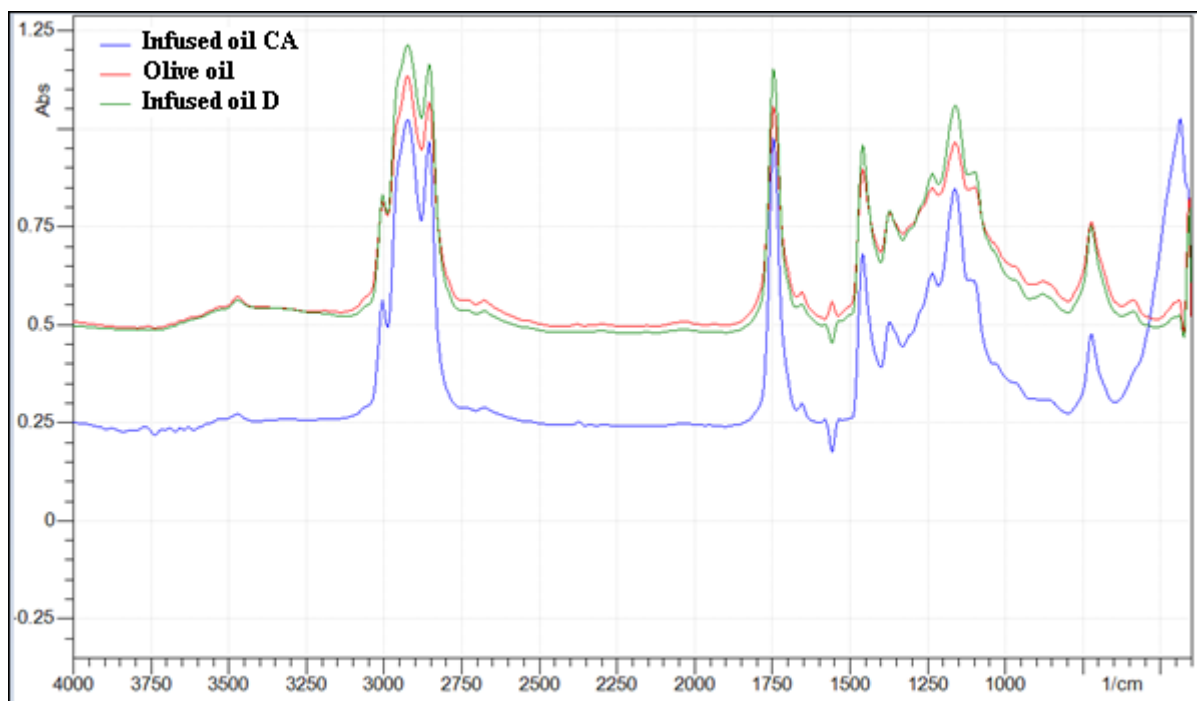


Figure 4: FTIR spectrum of the infused oils (CA and D) and olive oil

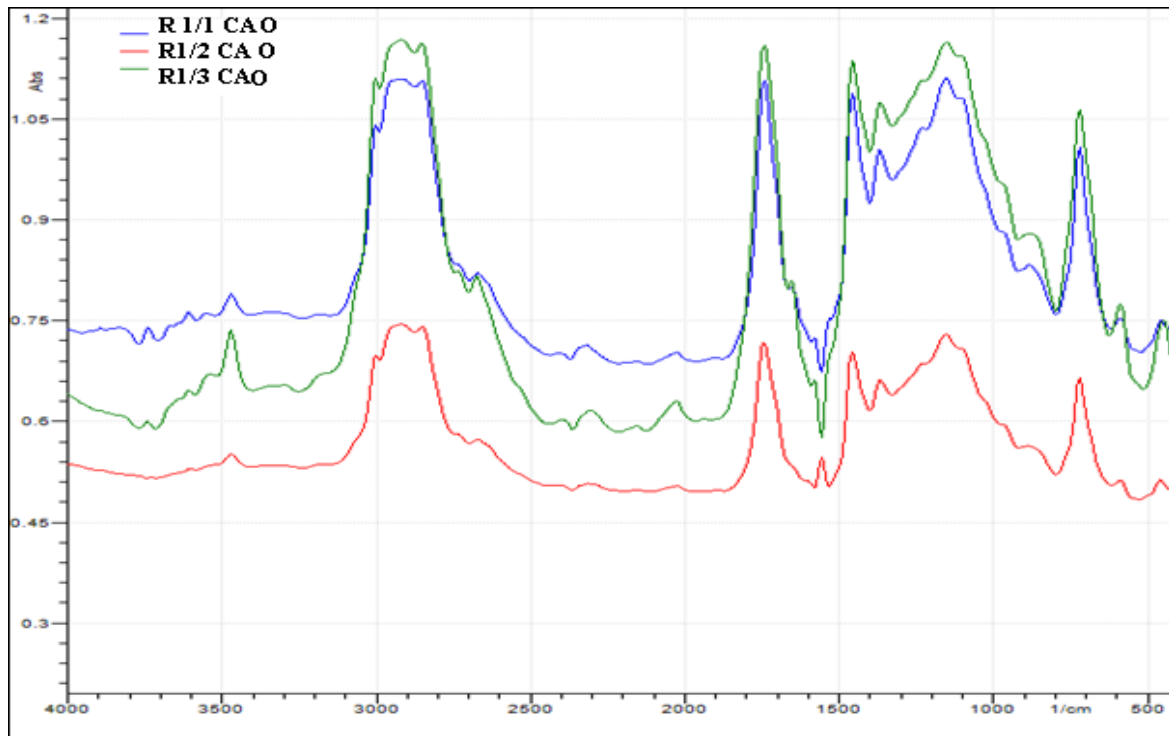


Figure 5: FTIR spectrum of the CAO

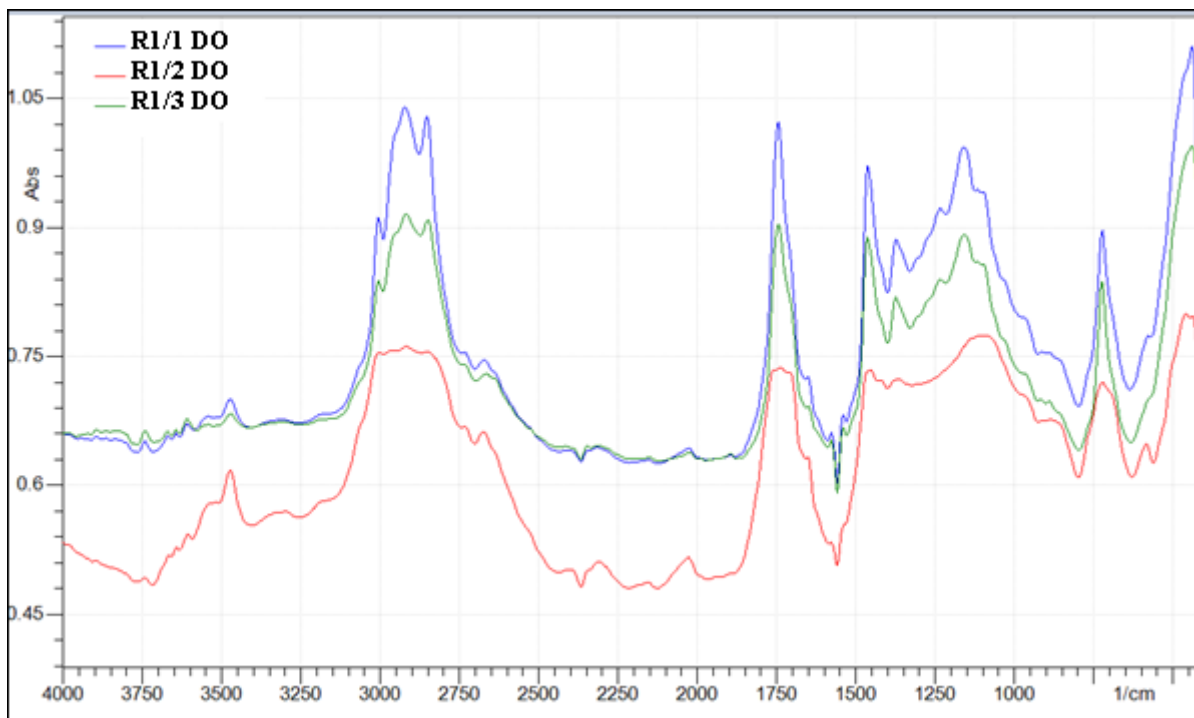


Figure 6: FTIR spectrum of the DO

## V. Conclusions

Through this study, we found that in the macroscopic characterization, a semi-solid consistency and homogeneity were attributed to our prepared ointments, the microscopic characterization of our ointments presents a better physical stability, the latter is characterized by a homogeneous

appearance, which was found for all the prepared ointments either for the yellow DO or orange CAO flowers. For the test of resistance to water, the ointment of ratio R (1/3) is considered the most resistant to it compared to the other ointments, which is explained by the presence of the

spherical shape of the deposited droplet. From the results obtained by chemical analysis, it is noted that the virgin oils spectra before and after infusion show the same appearance, however an increase in the intensities of the peaks for the infused oils compared to the virgin oil.

Concerning the comparison between the spectra of the orange CAO and yellow DO flower ointments, the R test (1/3) shows an increase in intensity in all its bands, which corresponds to the best chemical stability.

#### Acknowledgements

The authors would like to thank the students "LETRECHE Yasmina and BELAID Kahina" in pharmaceutical engineering of department of process engineering, university of Bejaia.

**Disclosure of interest:** The authors report no conflict of interest.

#### References

- [1] V. Schulz, R. Hänsel, V.E.Tyler. Rational Phytotherapy. A Physician's Guide to Herbal Medicine, 4th Ed., Berlin, Springer-Verlag. 2001.
- [2] D. Shaw. Risks or remedies ? Safety aspects of herbal remedies. Journal Royal Social Medicine, 91, 294–296, 1998.
- [3] F.A. Andersen, W.F. Bergfeld, D.V. Belsito, R.A. Hill, C.D. Klaassen,; D.C. Liebler, J.G. Marks, R.C. Shank, T.J. Slaga,; P.W. Snyder. Final report of the cosmetic ingredient review expert panel amended safety assessment of Calendula officinalis-derived cosmetic ingredients. International journal of Toxicology, 29, 221–243, 2010.
- [4] S. Stegemann, Patient centric drug product design in modern drug delivery as an opportunity to increase safety and effectiveness. Expert opinion on drug delivery, 15, 619–627, 2018.
- [5] S. Agatonovic-Kustrin, O.D. Babazadeh, D.W. Morton, A.P. Yusof. Rapid evaluation and comparison of natural products and antioxidant activity in calendula, feverfew, and German chamomile extracts. Journal of Chromatography, 1385, 103–110, 2015.
- [6] C. Ung-Kyu C, L. Ok-Hwan, Y. Joo Hyuk, C. Chang-Won, R. K. Young, L. SeongI, K. Young-Chan . Hypolipidemic and Antioxidant Effects of Dandelion (Taraxacum officinale) Root and Leaf on Cholesterol-Fed Rabbits. International journal of molecules science. 11, 67-78, 2010.
- [7] N.G. Bisset, M. Wichtl. Herbal Drugs and Phytopharmaceuticals: A Handbook for Practice on a Scientific Basis. CRC Press, 1994.
- [8] K. Schütz, R. Carle, A. Schieber. Taraxacum a review on its phytochemical and pharmacological profile. Journal of Ethnopharmacology, 107, 313–323, 2006.
- [9] H. J. Jeon, H. J. Kang, Jung, Y. S. Kang, C.J. Lim, Y. M. Kim, E. H. Park. Antiinflammatory activity of Taraxacum officinale. Journal of Ethnopharmacology, 115, 82–88, 2008.
- [10] C. A. Williams, F. Goldstone, J. Greenham. Flavonoids, cinnamic acids and coumarins from the different tissues and medicinal preparations of Taraxacum officinale. Phytochemistry 42, 121–127, 1996.
- [11] C. Hu, D. D. Kitts. Antioxidant, prooxidant, and cytotoxic activities of solvent-fractionated dandelion (Taraxacum officinale) flower extracts in vitro. Journal of Agricultural and Food Chemistry, 1, 51 (1), 301-10, 2003.
- [12] R. Bellache, D. Hammiche, A. Boukerrou. Prickly pear seed: from vegetable fiber to advanced applications: A review, Biopolymer applications journal. 1(1), 01-06, 2022.
- [13] M. D. Guillén and N. Cabo. Relationships between the Composition of Edible Oils and Lard and the Ratio of the Absorbance of Specific Bands of Their Fourier Transform Infrared Spectra. Journal of Agricultural and Food Chemistry, 46 (5), 1788-1793, 1998.

# An investigation of the mechanical properties of starch biofilms plasticized by glycerol

Aicha DEHANE<sup>1\*</sup>, Dalila HAMMICHE<sup>1</sup>, Amar BOUKERROU<sup>1</sup>, Balbir Singh KAITH<sup>2</sup>

<sup>1</sup>Laboratoire des Matériaux Polymères Avancés, Département Génie des Procédés, Faculté de Technologie, Université de Bejaia, Algérie.

<sup>2</sup>Department of Chemistry, Dr. B.R. Ambedkar National Institute of Technology, Jalandhar, Punjab-144011, India

Corresponding author email\* [aicha.dehane@univ-bejaia.dz](mailto:aicha.dehane@univ-bejaia.dz)

Received: 07 May 2022; Accepted: 07 June 2022; Published: 21 July 2022

## Abstract

*Within the framework of sustainable growth, the use of biodegradable polymers as an alternative to synthetic polymers seems to be the best solution that could resolve waste disposal problems. The aim of this work was to prepare a biofilm based on a biodegradable polymer: starch plasticized by glycerol. Different rate of glycerol are added in order to plasticize the starch (15%, 20% and 30%). The method used for this preparation was casting, the structural and mechanical analysis was carried out to investigate the addition effect on of this plasticizer on the mechanical and structural properties.*

**Keywords:** Starch, Glycerol, Biofilms, Plasticizer, Biopolymers, Flexibility.

## 1. Introduction

Numerous efforts have been made for replacement of synthetic polymers with relatively inexpensive, biodegradable, renewable and sustainable materials. These materials mainly include the chemically synthesized biopolymers such as poly (lactic acid) (PLA), poly (vinyl) alcohol (PVA), poly (caprolactone), poly (butylene) succinate; the microbially produced polymers such as polyhydroxy-butyrates (PHB), polyhydroxy-valerate and the naturally derived biopolymers such as starch, cellulose, chitosan, agar, gelatin, alginate etc. and their blends [1].

Among all natural materials, starch is a potential candidate to produce biodegradable polymers since it is renewable, biodegradable and abundantly available at low cost. Among the various type of starches, corn is the most predominant material constituting 73% of the main sources of starch produced worldwide, followed by cassava (14%), wheat (8%), potato (4%), and others (1%) [2].

Corn starch has the highest amylose content (28–33%), competing with wheat starch (30–32%) followed by potato (18–20%), and cassava starch (16–19%). Starch can be thermally processed to obtain thermoplastic starch using suitable plasticizer.

Starch is one of the most abundant polysaccharides (consists of two polymeric fractions: amylose and amylopectin), used in plastics industry, as eco-friendly, biodegradable alternative for oil-based materials, for example for paper processing and packaging [3]. Biopolymer films offer several advantages over conventional packaging material due to their excellent biodegradability, biocompatibility, and wide range of potential applications [4].

For instance, these films are capable to act as carriers for functional ingredients such as antimicrobial or antioxidizing agents, thus expanding their functionalities to be active packaging. Among many biopolymers, starch is a promising

alternative due to its availability, environmentally friendly, cost-effectiveness, and ease of handling [5].

More importantly, starch is able to be formed into transparent and odorless films without any chemical treatment requirement [6]. Nevertheless, native starch films present some limitations including the brittleness and hydrophilic nature [7], which have a direct impact on mechanical and barrier properties of the films and, thus affect the packaged food product [8]. These inherent properties can be solved with addition of plasticizers such as sorbitol, polyethylene glycol, and glycerol. Among the plasticizers, glycerol has often been used as plasticizer for starch films due to its compatibility with amylose [9], which promotes better mechanical properties by interfering with amylose packing, thereby decreases the intermolecular forces between the starch molecules. In turn, plasticized-starch films are more flexible and feasible for various packaging applications. Numerous studies have proved the effectiveness of glycerol as plasticizer in a concentration of 20–40% of the weight of starch [10].

For instance, Mali, Grossmann, García, Martino, & Zaritzky, 2006 has studied the effect of glycerol concentration (0, 20, 40%) on corn, tapioca, and yam starches. They revealed that, irrespective of the starch type, the tensile strength reduced while the elongation at break increased with the increase in glycerol concentration. This largely results from the interruptions of glycerol in the starch polymeric chains, creating more free volumes and reduce the glass transition temperature, which consequently improve the film softness and extensibility. A more recent work by Zahiruddin et al [11] reported that incorporation of 25% glycerol into tapioca starch film increased the elongation of the film by 4-fold and the film exhibited higher degradation temperature indicating better thermal stability. Similarly, Santana et al.[12] reported that 30% glycerol concentration had successfully improved the mechanical properties of

jackfruit seed starch film and yield moderate barrier properties. Furthermore, blending starch films with glycerol produces films that are more prone to water. Rodriguez et al [13] demonstrated how potato starch forms manageable films without the need to add plasticisers. However, their mechanical properties could be improved by adding glycerol (Gly), which was totally compatible with potato starch.

For instance, Orsuwan & Sothornvit [14], has incorporated glycerol into carboxylated styrene-butadiene rubber/cassava starch blend films. The water solubility and moisture content of the films were improved owing to the hydroxyl groups of glycerol that has high affinity to water molecules. They also found that addition of glycerol was able to increase the storage modulus of the starch film, which is desirable for use as food packaging. Overall, the presence of glycerol plays significant role in improving workability of starch films.

Glycerol is a potential bio-based material to afford prominent biocompatible yet biodegradable polymers for a variety of applications through direct polymerization, fermentation, and chemical conversion. Besides, glycerol plays a critical role in the food packaging industry to perform a plasticizing effect; it improves the ductility of the bio-derived packaging. The native unplasticized starch film is too brittle for handling, while the glycerol-plasticized starch film has adequate flexibility and processability, but with compromised water and gaseous barrier properties. Nevertheless, more established works should be published to exploit the use of this versatile base chemical in diverse fields to good advantages, yet reducing the adverse environmental impact [15].

In the present study, glycerol (fixed at 10%, 20% and 30% wt of corn starch) is dispersed. Corn starch (commercial), glycerol, is supplied by VWR, PROLABO Marketing. All chemicals were used as received without further purification.

## II. Materials and Methods

### II.1. Materials

- **The starch** : starch (commercial, cornstarch).
- **Glycerol** : was hunted down from VWR, PROLABO. It is a viscous, transparent, water-soluble liquid. (Chemical formula  $C_3H_8O_3$  Mn: 92.09 g/mol/ Density: 1.25 g/mL (at 25°C)/ Bp: 182°C /Mp: 20°C Flash point. 160°C).
- **Hydrochloric acid** : obtained from Sigma-Aldrich in a concentration of 37%,
- **Sodium hydroxide (NaOH)**. He was chased from Sigma-Aldrich.

### II.2. Methods

#### Preparation of films

Films based on corn starch (commercial, cornstarch) were prepared by casting, according to the experimental protocol described by Gao et al. [15] With the variation of plasticizer rate in the different films.

### Characterization of films

#### Fourier transform infrared (FTIR) spectroscopy

The chemical structures of the neat glycerol, neat starch and neat starch with different rate of glycerol (15%, 20% and 30%). were assessed by attenuated total reflectance-Fourier- transform infrared spectroscopy (ATR-FTIR) in an Alpha spectrometer (Bruker Optik GmbH, Ettlinger, Germany) using a germanium prism. Sixty scans were recorded and averaged at a resolution of 4  $cm^{-1}$  in the wavenumber range 4,000–400  $cm^{-1}$ . Under these experimental conditions, a depth of the surface of about 1  $\mu m$  was analyzed.

#### Mechanical properties

The tensile strength (TS); tensile strain and elongation at break (EB) of the starch-based film with different rate of glycerol are added in order to plasticize the starch (15%, 20% and 30%).

Specimens were determined by a ZWICK ROELL universal tensile machine with test control II load cell 500N. Classe extensometer 1; preload 1N test speed 100mm/min; traction module speed 1mm/min; with an initial grip separation of 72.82 mm at a speed of 100 mm/min [16]. All films were cut into strips (125 mm  $\times$  20 mm) and equilibrated at a temperature of  $23 \pm 2$  °C and relative humidity of 53% for at least 72 h before testing

## III. Results and discussion results

### III.1. Chemical properties of films

Based on Figure 1, the FTIR spectrum of the TPS shows all film specimens exhibited characteristic peaks belonging to starch. The peaks at 2920 and 1640  $cm^{-1}$  were related to C–H stretching vibration and tightly bound water bending vibration, respectively [17]. A broad peak at approximately 3280  $cm^{-1}$  was attributed to complex stretching vibrations of hydroxyl groups that were associated with the formation of inter- and intramolecular hydrogen bonds [18].

Thus, the hydroxyls of glycerol are bound together or with those carried by the structure of the starch via hydrogen bridges, causing, consequently a notorious intensification of the mass due to the bound OH which confirms by the increase in the intensity the band of the C–O–H group at about 1005  $cm^{-1}$  from the 20% glycerol formulation. Demonstrated the effects of this percentage of glycerol in starch films that reduced interactions of hydroxyl groups in the starch matrix with creation of Intermolecular hydrogen bonding existed between glycerol and starch via hydroxyl groups of glycerol, starch.

This shift confirmed that plasticizer could disrupt the intermolecular and intramolecular hydrogen bonding between starch molecules and then facilitate the movement of starch chains, which is beneficial for the formation of

stronger hydrogen bonds between starch molecules and plasticizer [19]. The water absorbed by the starch is also detected thanks to the valence vibration of the O-H bond of the H-O-H group observed around 1640 cm<sup>-1</sup>. The band

located around 1425cm<sup>-1</sup> corresponds to the deformations of the C-H groups – CH<sub>2</sub>-. Absorptions observed between 859 and 550 cm<sup>-1</sup> are due to strain vibrations of the C–H bonds of starch.

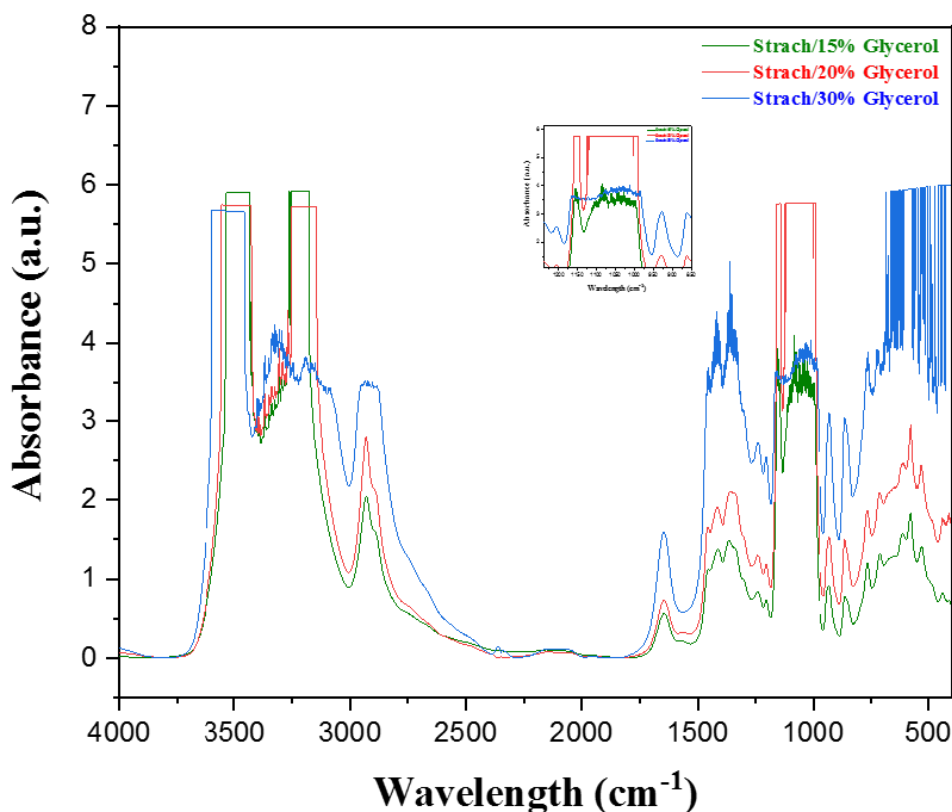


Figure 1: FT-IR spectra of starch-based films plasticized with glycerol (G) at different proportions of 30% G (a), 20% G-10%.

### III.2. Mechanical properties

Mechanical properties of packaging material are crucial to evaluate the strength and durability of the material to package products and withstand extraneous forces.

Tensile strength (TS) and elongation at break (EAB) values denote the ability of food packaging film to retain its integrity under tensile stress during processing, handling, and storage [20] while Young's modulus (YM) values indicate stiffness of the material.

Figure 2. illustrates the effects of adding glycerol on the Stress, Tensile strength, Elongation at Break, Toughness and Elasticity modulus of neat starch films.

Figure 2 (a) shows the effect of glycerol on YM /TS of CS films. It can be seen that the trend of the results is similar to that of TS.

Tensile properties TS is the maximum amount of tensile stress the material can withstand before failure. On the other hand, E is an extension under tension, reflecting the elasticity of a material [20]. The results showed that the tensile properties of films starch plasticized by glycerol were in addition, films at 20% Gly showed a significantly stronger value Ts compared to films with 30% and 10 Gly. Chang et al. [22] have already pointed out the close relationship between the film the glycerol content and the mechanical

properties of the film. In other words, the presence of the 20% glycerol in the CS film formulation increased the YM more intensely compared to the effect of 10 and 30 glycerol on the other hand when we compare YM and TS between the formulation of 10% and 30% we find that the presence of glycerol significantly reduces the YM from CS movie respectively.

This finding can be associated with the hygroscopic character of the glycerol possessed by the several hydroxyl groups, which enhanced the ability of starch films to hold water. This consequently reduced the rigidity of the indicated films by drastically reducing YM while increasing softness and flexibility. This finding is similar to Mali et al. [10] who studied the effect of different concentrations of glycerol on maize starch films. They found that corn starch film reduced YM by 1188 at 551 MPa and 139 MPa, with the addition of 20% and 40% glycerol.

Figure 2 (b) shows the effect of glycerol on the EAB/Toughness of CS film. respectively. The presence of glycerol led to the mobility of the CS polymeric chain, thus under applied stress, the flexibility and elasticity of the CS film increased significantly.

For example, Lourdin et al. [23] reported that a small amount of plasticizer can easily insert between the polymer chains, which increases the free volume and mobility of the polymer chains and improves their extensibility. Similar results have been previously reported for hydroxypropil starch films by Arvanitoyannis et al [24].

If we undergo the elongation at break, we see that the value of the breaking stress at 20% glycerol increases, which is in contradiction with what is generally observed. One could conjecture that our films are quite ductile; On the other hand, the films are more ductile, resulting in easy breakage.

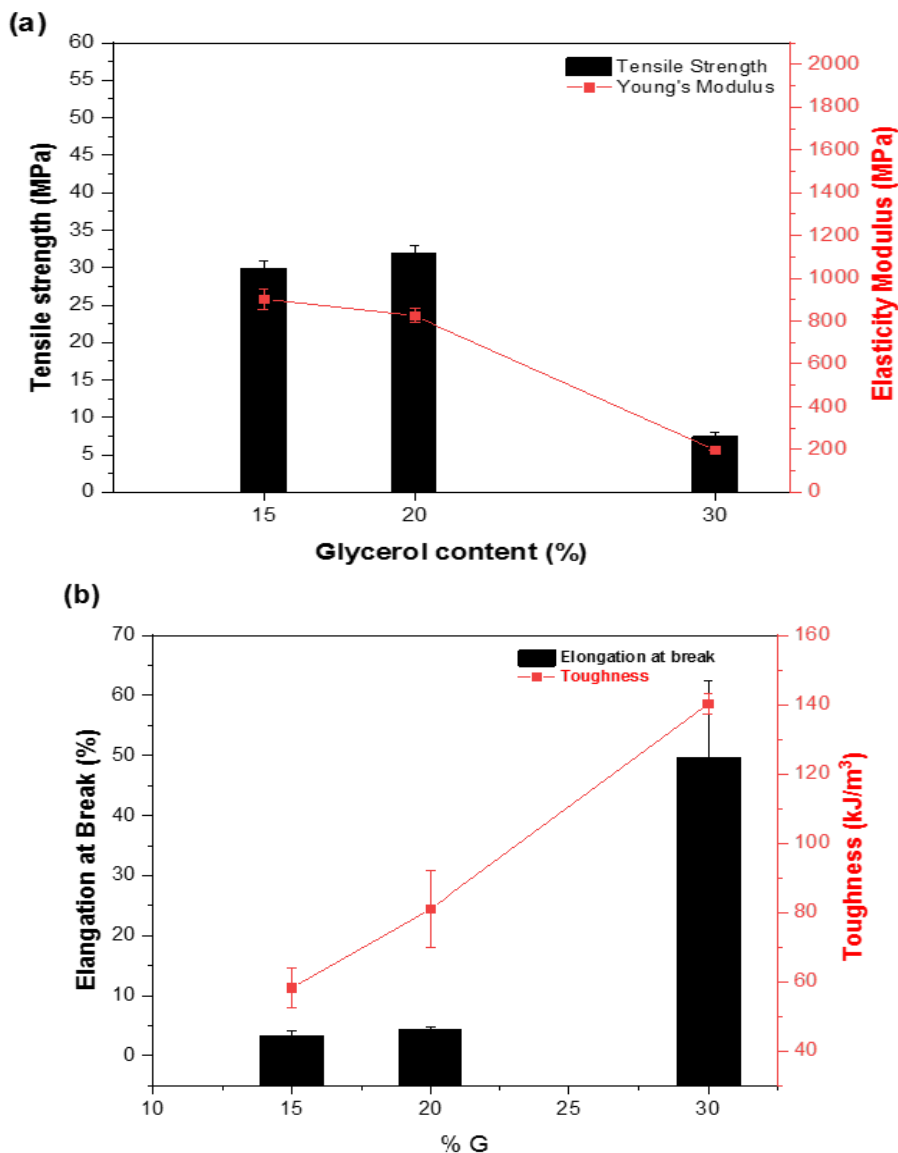


Figure 2: Mechanical properties of corn starch films containing glycerol (10%, 20% and 30%): (a) TS and YM. (b) EAB and toughness.

The study of the mechanical behavior in tension consists in following the shape of the stress-strain or force-elongation curves and in comparing the behavior in tension of the samples studied.

The force-elongation curves of our samples are represented in the Figure 3, there are two zones: We note that the behavior of the films is qualitatively almost identical in the first zone.

- Zone 1 (linear part): This zone represents the linear elastic zone, in which a release of the load results

immediately in a full recovery. According to Oudet (1986), the deformation in this zone is probably due to the deformation of the valence angles superimposed on the movements of some chains of the amorphous domain. In this zone, stress and strain are related by Hooke's law.

- Zone 2 only for the formulation of 30% glycerol: in this zone, we notice a drop in the force (stress) as a function of the elongation (deformation) due to the onset of rupture of intermolecular bonds of the hydrogen type for the essential. This zone is qualified as zone of plastic deformation, where this

one is permanent there and a relaxation of the stress does not involve any recovering.

Figure 3 shows some representative stress-strain curves for 10% and 20% starch /glycerol samples. It is clear that Figure vs exhibits typical brittle fracture behavior [25] described by

relatively high tensile strength, low percentage of elongation and no elastic limit, whereas at high glycerol content a marked increase in the percentage an elongation was observed accompanied by a very clear elastic limit Figure vs. for 30% formulation.

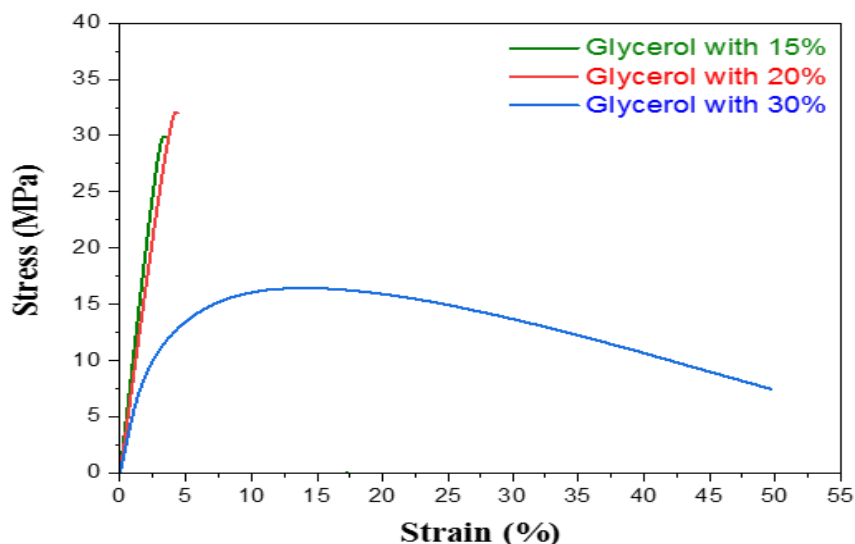


Figure 3: Effect of the price of glycerol content on the stress of starch/glycerol in terms of strain.

#### IV. Conclusions

Films of starch plasticized by deferent glycerol content have been prepared and their mechanical and chemical properties have been studied. FTIR spectroscopy indicated that the interactions occurred between the hydroxyl groups in the matrix of the starch/glycerol biofilms, case of the 20% glycerol formulation. The elongation at break of the biofilms increased significantly with increasing glycerol, also the tensile strength of the 20% glycerol formulation increased by a poorer 10% and 30% formulation. Therefore, we can see several changes in mechanical chemical properties when we change the level of glycerol so to make a specific application it is necessary to optimize the percentage of plasticizer.

#### Acknowledgments

The authors are very grateful to the students in Polymer engineering of the University of Bejaia.

**Disclosure of interest:** The authors report no conflict of interest.

#### References

- [1] M. S. Sarwar, M. B. K. Niazi, Z. Jahan, T. Ahmad, A. Hussain. Preparation and characterization of PVA/nanocellulose/Ag nanocomposite films for antimicrobial food packaging, *Carbohydrate Polymers*. 184, 453–464, 2018.
- [2] A. Torres, S. Li, S. Roussos, M. Vert. Poly(lactic acid) degradation in soil or under controlled conditions, *Journal of Applied Polymer Science*. 62(13), 2295–2302, 1996.
- [3] A. Kraak. Industrial applications of potato starch products, *Industrial Crops and Products*. 1, 107-122, (1992).
- [4] J. W. Rhim, P. K. Ng. Natural biopolymer-based nanocomposite films for packaging applications, *Critical Reviews in Food Science and Nutrition*. 47(4), 411–433, 2007.
- [5] S. H. Othman, N. A. Majid, I. S. Tawakkal, M. A. Basha, R. K. Nordin, R. Shapi'i Ahmad. Tapioca starch films reinforced with microcrystalline cellulose for potential food packaging application. *Food Science and Technology*. 2019.
- [6] W. T. Owi, O. H. Lin, S. T. Sam, A. R. Villagracia, G. N. C. Santos. Tapioca starch based green nanocomposites with environmentally friendly cross-linker. *56*, 463–468, 2017.
- [7] F. M. Pelissari, M. V. Grossmann, F. Yamashita, E. A. G. Pineda. Antimicrobial, mechanical, and barrier properties of cassava starch-chitosan films incorporated with oregano essential oil, *Journal of Agricultural and Food Chemistry*. 57(16), 7499–7504, 2009.
- [8] R. A. Shapii, S. H. Othman, M. N. Naim, R. Kadir Basha. Mechanical properties of tapioca starch-based film incorporated with bulk chitosan and chitosan nanoparticle: A comparative study. *Pertanika Journal of Science and Technology*, 27 (S1), 95–107, 2231–8526, 2019.
- [9] M. G. A. Vieira, M. A. da Silva, L. O. dos Santos, M. M. Beppu. Natural- based plasticizers and biopolymer



- films: A review, *European Polymer Journal*. 47(3), 254–263, 2011.
- [10] S. Mali, M. V. E. Grossmann, M. A. García, M. N. Martino, N. E. Zaritzky. Effects of controlled storage on thermal, mechanical and barrier properties of plasticized films from different starch sources, *Journal of Food Engineering*. 75(4), 453–460, 2006.
- [11] S. M. M. Zahiruddin, S. H. Othman, I. S. M. A. Tawakkal, R. A. Talib. Mechanical and thermal properties of tapioca starch films plasticized with glycerol and sorbitol. *Food Research*, 3(2), 157–163, 2019.
- [12] R. F. Santana, R. C. F. Bonomo, O. R. R. Gandolfi, L. B. Rodrigues, L. S. Santos, A. C. dos Santos Pires. Characterization of starch-based bioplastics from jackfruit seed plasticized with glycerol. *Journal of Food Science & Technology*, 55 (1), 278–286, 2018.
- [13] M. Rodriguez, J. Ose's, K. Ziani, J.I. Mate. Combined effect of plasticizers and surfactants on the physical properties of starch based edible films, *Food Research International*. 39, 840–846, 2006.
- [14] A. Orsuwan, R. Sothornvit. Effect of banana and plasticizer types on mechanical, water barrier, and heat sealability of plasticized banana-based films, *Journal of Food Processing and Preservation*. 42(1), e13380, 2018.
- [15] W. Gao, P. F. Liu, X. Y. Li, L. Z. Qiu, H. X. Hou, B. Cui. The co-plasticization effects of glycerol and small molecular sugars on starch-based nanocomposite films prepared by extrusion blowing, *International Journal of Biological Macromolecules*. 133, 1175–1181, 2019.
- [16] W. Gao, H. Z. Dong, H. X. Hou, H. Zhang. Effects of clays with various hydrophilicities on properties of starch-clay nanocomposites by film blowing, *Carbohydrate Polymers*. 88, 321–328, 2012.
- [17] B. Zhang, J. Q. Mei, B. Chen, H. Q. Chen. Digestibility, physicochemical and structural properties of octenyl succinic anhydride-modified cassava starches with different degree of substitution, *Food Chemistry*. 229, 136–141, 2017.
- [18] A. Jimenez, L. Sánchez-González, S. Desobry, A. Chiralt, E. A. Tehrany. Influence of nanoliposomes incorporation on properties of film forming dispersions and films based on corn starch and sodium caseinate. *Food Hydrocolloids*, 35, 159–169, 2014.
- [19] A. A. Ahmet, V. Ilberg. Effect of different polyol-based plasticizers on thermal properties of polyvinyl alcohol: Starch blends films. *Carbohydrate Polymers*, 136, 441–448, 2016.
- [20] S. Salmieri, F. Islam, R. A. Khan, F. M. Hossain, H. M. Ibrahim, C. Miao. Antimicrobial nanocomposite films made of poly (lactic acid)–cellulose nanocrystals (PLA–CNC) in food applications-Part B: Effect of oregano essential oil release on the inactivation of *Listeria monocytogenes* in mixed vegetables. *Cellulose*, 21(6), 4271–4285, 2014.
- [21] F. E. Silva, M. C. Leal, B. D. M. Batista, K. D. A. Fernandes. PVA/ polysaccharides blended films: Mechanical properties. *Journal of Materials*. pp. 1–5, 2013.
- [22] Y.P. Chang, A.A. Karim, C.C. Seow. Interactive plasticizing- antiplasticizing effects of water and glycerol on the tensile properties of tapioca starch films. *Food Hydrocolloids*, 20, 1–8, 2006.
- [23] D. Lourdin, H. Bizot, P. Colonna. Influence of equilibrium relative humidity and plasticizer concentration on the water content and glass transition of starch materials. *Polymer*, 38(21), 1047 – 1053, 1997.
- [24] I. Arvanitoyannis, & C.G. Biliaderis, Physical properties of polyol-plasticized edible films made from sodium caseinate and soluble starch blends. *Food Chemistry*, 62, 333–342. Arvanitoyannis, I., Nakayama, A. & Aiba, S. (1998). Edible films made from hydroxypropyl starch and gelatin and plasticized by polyols and water. *Carbohydrate Polymer*, 36, 105–119, 1998.
- [25] D.W. Van Krevelen. *Properties of Polymers*, Amsterdam: Elsevier 3rd ed, pp. 189-225, 1990.

# Perfection of a composite material reinforced by a natural filler modified by a gamma irradiation treatment

Nadira BELLILI<sup>1,2\*</sup>, Badrina DAIR<sup>1,2</sup>, Noura HAMOUR<sup>2</sup>, Hocine DJIDJELLI<sup>2</sup>, Amar BOUKERROU<sup>2</sup>

<sup>1</sup>Department of Petrochemical and Process Engineering, Faculty of Technology, Skikda University 20Aout – 1955 – Algeria.

<sup>2</sup>Department of Process Engineering, Faculty of Technology, Laboratory of Advanced Polymer Materials (LMPA), Abderrahmane MIRA University, Béjaïa, Algeria

\*Corresponding author email: dina\_1961s@yahoo.fr; n.bellili@univ-skikda.dz

Received: 9 May 2022; Accepted: 2 July 2022; Published: 21 July 2022

## Abstract

*Olive residue flour (ORF) were irradiated at doses of 10, 25, 50 and 70 (kGy) and incorporated in Poly (vinyl chloride) (PVC) in different ratios of 10/90 and 20/80 (wt ORF %/PVC wt%) for the preparation of composites. Mechanical behaviors of those composites such as tensile strength and elongation at break have been, assessed. The composite samples prepared with the untreated filler present a decrease of elongation and tensile strength. This decrease is, attributed to the low interfacial adhesion between the filler, which have a strong affinity for water (hydrophilic strength) and the PVC hydrophobic surface. However, the composite filled with ORF treated with gamma irradiation exhibit higher elongation and tensile strength than those of un-irradiated composites. This is, attributed to the decrease in the hydrophilicity of the olive residue flour after gamma-irradiation treatment. The results of the mechanical behavior shown by the structure morphology observation indicate an improvement of the ORF dispersion as seen through Scanning Electron Microscopy. The water-absorption test of different composites shows that irradiated filler composites present less water uptake than those of unirradiated composite.*

**Keywords:** Poly (vinyl chloride), wood flour, wood plastic composite,  $\gamma$ -radiation

## I. Introduction

Lignocellulosic fibers are, used as fillers or reinforcements in composites with thermoplastic matrices for industrial applications. In fact, hydrophilic character of these lignocellulosic materials disrupts the preparation of such materials based a thermoplastic matrix with a hydrophobic nature giving poor interfacial compatibility, which causes poor mechanical properties.

The industry of olive oil Algerian produces about 200,000 tons of solid waste and the amount tends to increase each year [1]. Chemically, olive residue flour constitutes the cellulose, hemicellulose and lignin and in order to reduce the hydrophilicity of the flour to improve the addition force to the thermoplastic matrix, it is necessary to perform a structural modification of this surface. Several approaches have been studied, Djidjelli, H. et al. have carried out the plasticization of olive residue flour by benzyl chloride to improve some thermal and physicochemical properties of composite PVC/olive residue flour [2]. Boukerrou A. et al. have decreased hydrophobicity of olive residue flour by silanization of the latter [3]. Another technique, which is simpler and less expensive based on the gamma irradiation of composites.

This technique, has been used by several researchers in indeed, Khan M. A. et al. have studied the effect of the filler and the matrix treatment by gamma radiation on the properties of composite [4]. Cemmi A. et al. have succeeded to decrease the wettability of the cellulose by gamma irradiation [5].

In this work, olive residue flour has been irradiated with gamma radiation at doses of 10, 25, 50, 60 and 70 (kGy) and the composites based on polyvinyl chloride (PVC) loaded with 10 and 20% in weight of filler treated and untreated were prepared. The mechanical and morphological characteristics of PVC composites/FGO were studied and the rate of water absorption was determined.

## II. Material and methods

### II.1. Materials

Olive residue flour was used as filler having a diameter of around 100 ( $\mu\text{m}$ ), it was collected from Bejaia, Algeria. ORF was dried at 100 °C in a vacuum oven for 24h prior to the preparation of the composites. The matrix in this work was based on PVC type 3000H produced by CIRES (USA). The polymer has the following physical characteristics: Kw value: 72; powder, density: from 0.48 to 0.56 (g.cm<sup>-3</sup>). The additives used in the preparation of the various formulations are dioctyl phthalate (DOP) as a plastizer with a viscosity range from 75-80 CSt, a molecular weight of 390 (g.mol<sup>-1</sup>), a boiling temperature of 231°C. Ca/Zn type Lankromark LC486 produced by Akros Chemicals, and stearic acid were also used as stabilizer and lubricant respectively. The mass composition of the different formulation is, summarized in Table 1.

**Table 1.** Mass composition of formulation for PVC/ Olive residue flour

Compounds	Resin of PVC	Plasticizer	Ca/Zn	Stearic acid
F0 (grams)	100	30	2	0.6
F10(grams)	90	30	2	0.6
F20(grams)	80	30	2	0.6

## II.2. Pretreatments of olive residue flour

The Algerian, olive residue flour was, subjected to several pretreatments: washing with hot water to eliminate pulp, drying under ambient conditions for 48 h, and then drying in an oven at 105 °C for 24 hours. The powder was then subjected to crushing and finally sifting to obtain a flour of size smaller than 100 (µm). The flour of olive residue obtained was then washed with acetone in a soxhlet extractor for 24 hours to eliminate any contamination or impurity.

## II.3. Irradiation treatment

ORF was treated with γ-rays from a 60Co source in air at room temperature at doses of 10, 25, 50 and 70 kGy using a dose rate of 48 (kGy/h).

## II.4. Sample preparation

The mass composition of the pure PVC (F0), PVC/olive residue (F10) and (F20) formulations is represented in Table 1. Sheets with a thickness about 1mm are obtained by a calendaring process at 160 °C and a residence time of 15 min.

## III.Characterization of composites

### III.1. Mechanical properties of composites

Specimens for mechanical testing were prepared in accordance with standard CEI 60811-1-1. , type "H" have the following dimensions Figure1. Tests were carried out using a tensile testing machine of type: BTC-FR 2.5TN.D09, at room temperature. The tensile speed was 100 (mm/min). The reported data are the average of five successful tests.

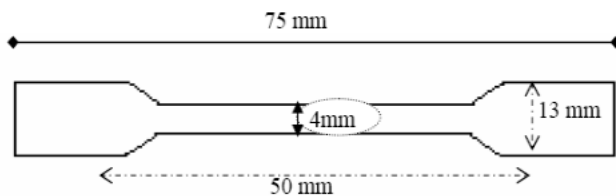


**Figure 1.**The "H" type specimen

### III.2. Surface morphology

Scanning electron microscopy (SEM) was, used to examine qualitatively the dispersion of lignocellulosic fibers in the PVC matrix. The surface of the composites was, examined with a Philips scanning electron microscope.

## III.3. Water-absorption tests

Water absorption of composite was, examined by immersion of sheet sample of 1mm thickness in distilled water at room temperature for 24 h, periodically measuring the change in weight of the sample. After weighing, the WA of the samples was, calculated as eq. (1).

$$W_A(\%) = \left( \frac{W_t - W_0}{W_0} \times 100 \right) \quad eq. 1$$

Where  $W_0$  and  $W_t$  are the weights of the sample before and after immersion in distilled water, respectively

## IV.Results and discussion

### IV.1. Effect of untreated ORF, on mechanical and morphology properties of composites (Tensile properties)

The values of elongation at break, tensile strength and the Young's modulus for the composites were, measured and the results were, summarized in Table 2. It is, observed that the tensile strength and elongation at break decreases. These results were in accordance with much work [6-8], that has attributed this decrease to the low interfacial adhesion between the filler and the polymer matrix. Wood materials have a strong affinity for water (hydrophilic strength) which creates an incompatibility interface between it and the PVC hydrophobic surface. The deterioration of the elongation at break is also partially due to the incorporation of the rigid flour into the matrix of the PVC, which reduces the mobility of the polymeric chains and facilitates the break of the specimen at low stress.

The incorporation of the ORF into the matrix significantly improves the Young's modulus compared to that for PVC alone. This can be, explained by the fact that the particles of ORF have a rigid character leading to a high resistance to deformation.

**Table 2.** Stress (σ) and the elongation at break (ε) values for F0, F10 and F20

Compounds	F0	F10	F20
Strength at break σ (MPa)	24.24±3.70	20.60±2.23	16.91±2.77
Elongation at break ε (%)	124.27±2.63	74±1.26	43.82±03.12
Young's modulus E (MPa)	189,41±1,90	192±1,05	193±2,83

### Effect of ORF on morphology of composites

The morphological of the fracture surfaces of F0, F10 and F20 composites investigated by SEM are, shown in Figure 2.

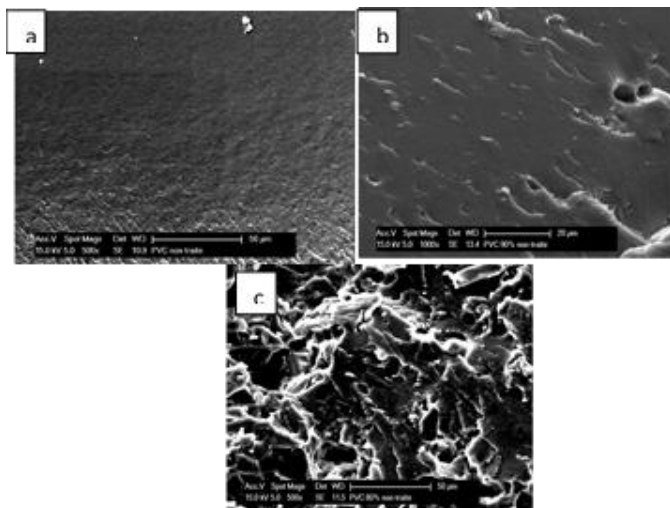


Figure 2. Scanning electron micrograph of: (a) F0, (b) F10, (c) F20

Figure 2a shows the SEM image of freeze-fractured F0 sample. A uniform structure of PVC is displayed. Observing Figure 2b and Figure 2c corresponding to the morphological of the fracture surfaces of F10 and F20 composite we notice a

rough morphology and many gaps and voids. This indicates poor interfacial adhesion that reveals the low affinity between the polymer matrix and the ORF fiber. Poor interfacial adhesion seems to facilitate debonding of the fiber [9].

### Effect of gamma radiation on the mechanical properties of ORF in PVC composites Tensile properties

ORF was, treated with  $\gamma$ -rays at doses of 10, 25, 50, and 70 (kGy) and incorporated in PVC to enhance the composites properties. Figure 3.a and Fig.3.b show the tensile strength and elongation at break as a function of radiation doses of composites.

For F10 composite, the results shown that the strength at break increases at dose of 10 (kGy), after that, it remains almost constant by increasing the radiation dose to 70 (kGy). The elongation at break increases with increasing irradiation dose. For F20 composite, the tensile strength increases by increasing the radiation dose to 70(kGy) and the elongation at break increases from 10 to 50 (kGy) dose and after that the value of elongation at break decreases up to 70 (kGy) dose, but it remains higher than that of untreated composite.

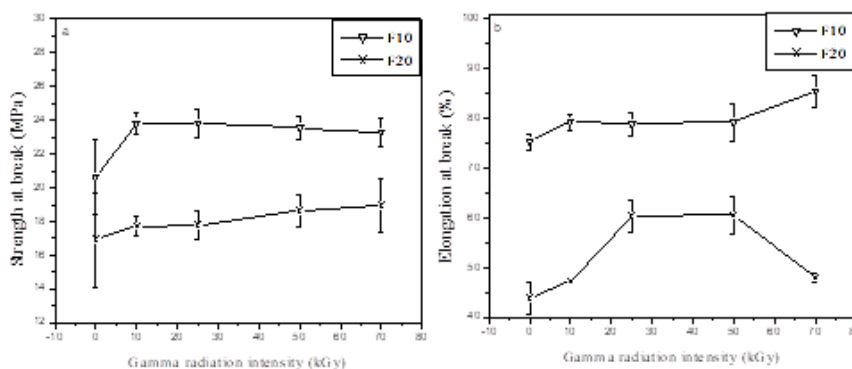


Figure 3. Effect of gamma radiation dose on: (a) tensile strength, (b) elongation at break of composites

The best mechanical properties were obtained for F10 composite irradiated at 70 kGy, we found that the tensile strength = 23.83 MPa, and elongation at break = 85.42%.

The improvements of tensile strength and elongation at break doses may be due to the intercross-linking between the neighboring cellulose molecules that occurs under gamma exposure [10, 11].

### IV.2. Morphology

To verify the results of the tensile test, we have analyzed various samples by SEM and the micrographs of the fracture surfaces of F10 before and after treatment at doses of 10 and 70 (kGy) doses are, shown in Figure 4.

Where F10 10kGy: PVC filled with 10% of ORF irradiated at dose of 10 (kGy), and F10 70kGy: PVC filled with 10% of ORF irradiated at dose of 70 (kGy).

Dispersion of the filler in the un-irradiated composites is, presented in Figure 4a. Some cavities are to be, seen where the

filler has been pulled-out. The presence of these cavities means that the interfacial bonding between the filler and the matrix polymer is poor and weak.

This is due to the presence of the polar, hydroxyl groups on the surface of lingo-cellulose, the major component of the flour of olive residue, which resulted in agglomeration and the poor adhesion with the non-polar PVC [12-14]. Figure 4b and Fig.4c show the micrographs of the fracture surfaces of irradiated composites at doses of 10 and 70 kGy respectively. Fewer cavities are presents compared the un-irradiated composite surface. This indicates that the interfacial bonding between filler and matrix is generally, improved after gamma irradiation. The best result was, obtained with the composite irradiated with a dose of 70 (KGy).

In addition, cracks between the filler and the matrix are apparent in these figures. The cracks and pores left from pulled-out filler can easily be, seen. Under high, energy radiation ionized and excited molecules are, formed. The polymer may undergo scission to be broken into smaller

fragments or else cross-linking, or the molecules may be linked together into large molecule. In fact, the free radicals thus produced may react to change structure of the polymer and alter the physical properties of the materials [10, 11].

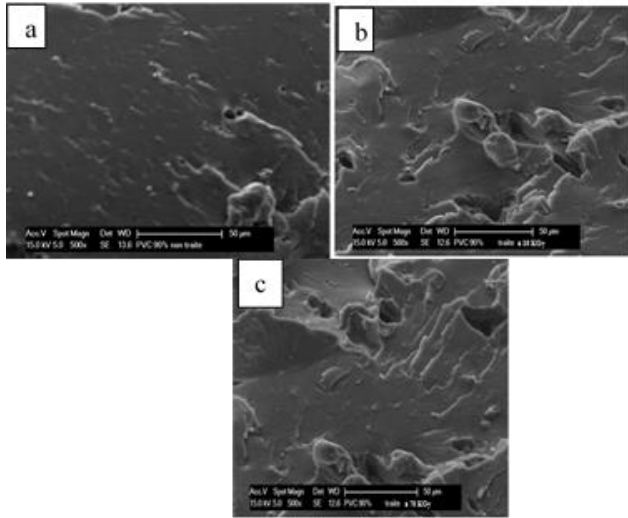


Figure 4. Scanning electron micrograph of a: F10, b: F10 10kGy, c: F10 70kGy

### IV.3. Water absorption

The results of water absorption are, shown in Figure 5. It is recognized that the absorption of water by different composites is largely dependent on the availability of free-OH groups on the surface of reinforcing fibers. Therefore, it is evident in the figure that WA (%) increases with an increase in filler loading. With an increase in filler loading, the number of hydroxyl groups in the composites increases, which consequently increases the WA. The water absorption results demonstrated that the composites filled with gamma irradiated ORF absorbs less amount of water. A lower absorption of water by the composite indicates that more OH groups of cellulose are, blocked from their interaction with PVC matrix. It is, also believed that -OH groups of cellulose molecules in the composites are mutually bonded or cross-linked due the effect of  $\gamma$ -radiation [10].

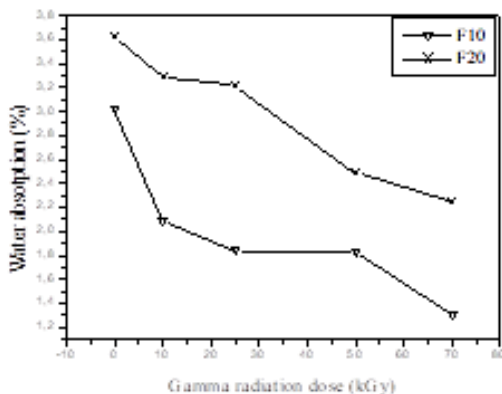


Figure 5. Water absorption of the various composites

### V. Conclusion

The purpose of this study was to investigate the effect of ORF and gamma irradiation on mechanical and morphological properties of a composite PVC/olive residue flour. The presence of olive residue flour with hydrophilic nature in the hydrophobic PVC matrix, leads to a material characterized by a heterogeneous dispersion and a weak interfacial adhesion. Gamma radiation treatment at low doses improve the mechanical performance of the ORF reinforced PVC composite, and a lower absorption of water by the composite filled with gamma irradiated ORF was observed. The improvement interaction between flour of olive residue and PVC by radiation treatment is, also verified from the SEM of fracture surface of the composite, by the reduction in the cavities on the surface.

Define abbreviations that are not standard in this field in a footnote to be placed on the first page of the article. Such abbreviations that are unavoidable in the abstract must be defined at their first mention there, as well as in the footnote. Ensure consistency of abbreviations throughout the article.

**Conflict of interest.** The authors report no conflict of interest.

### References

- [1] R. Derriche, K.S. Berrahmoune. Valorization of olive oil cake by extraction of hemicelluloses. *Journal of Food Engineering*, 78, 1149 -1154, 2007.
- [2] H. Djidjelli, D. Benachour, A. Boukerrou, O. Zefouni, J. Martinez-Véga, J. Farenc, M. Kaci. Thermal, dielectric and mechanical study of poly (vinyl chloride)/olive pomace composites. *Express Polymer Letter*, 12, 846-852, 2007.
- [3] A. Boukerrou, S. Krim, H. Djidjelli, C. Ihamouchen, J.J. Martinez. Study and characterization of composites materials based on polypropylene loaded with olive husk flour. *Journal of Applied Polymer Science*, 122, 1382-1394, 2011.
- [4] A .M. Khan, A. R. Haydaruzzaman, A.H. Khan, M.A. Hossain. Effect of gamma radiation on the performance of jute fabrics-reinforced polypropylene composites. *Radiation Physics and Chemistry*. 78, 986-993, 2009.
- [5] A. Cemmi, S. Baccaro, M. Carewska, C. Casieri, A. Lepore. Structure modifications and interaction with moisture in  $\gamma$ -irradiated pure cellulose by thermal analysis and infrared spectroscopy. *Polymer Degradation and Stability* 98, 2005-2010, 2013.
- [6] D. Maldas, B.V. Kokta, R.G. Raj, S.T. Sean. Use of wood fibers as reinforcing fillers for polystyrene. *Material Science and Engineering A*, 104, 235-244, 1988.
- [7] D. Kamdem, H.,Jiang, Development of Poly (vinyl chloride)/Wood Composites. A Literature Review. *Journal of Vinyl and Additive Technology*, 2, 59-69, 2004.
- [8] R. Mulhaupt, F. Stricker, M. Bruch. Mechanical and thermal properties of syndiotactic polypropene filled with glass beads and talcum. *Polymers*, 38, (21), 5347-5353, 1997.
- [9] K. Wang, Y. Zhao, F. Zhu, P. Xue, M. Jia. Properties of poly (vinyl chloride)/wood flour/montmorillonite

- composites: Effects of coupling agents and layered silicate. *Polymer Degradation and Stability*, 91, 2874-2883, 2006.
- [10] D. Bhattacharyya, X., Yuan, K. Jayaraman. Effects of plasma treatment in enhancing the performance of wood fiber-polypropylene composites. *Composites: Part A*, 35, 1363-1374, 2004.
- [11] S. Kalia, K. Thakur A. Celli, M. A. Kiechel, C. L. Schauer. Surface modification of plant fibers using environment friendly methods for their application in polymer composites, textile industry and antimicrobial activities: A review, *Journal of Environmental Chemical Engineering*, 1, 97-112, 2013.
- [12] M. Marcus, R. Itana, G. Timo, K. Andreas. Influence of various wood modifications on the properties of polyvinyl chloride/wood flour composites. *Journal of Applied Polymer Science*, 125, 308-312, 2012.
- [13] Y.Z. Meng, X.C. Ge, X.H.J. Li. Tensile properties, morphology, and thermal behavior of PVC composites containing pine flour and bamboo flour. *Journal of Applied Polymer Science*, 93, 1804-1811, 2004.
- [14] D.P. Kamdem, H. Jiang. Thermal and dynamic mechanical behavior of poly (vinyl chloride)/wood. *Journal of Applied Polymer Science*, 107, 951-957, 2008.

# Safranin dye degradation by using Fe<sub>2</sub>O<sub>3</sub>-SnO<sub>2</sub> Nanocomposites under natural Sunlight

Ganesh Kavita Parshuram JADHAV<sup>1</sup>, Omkar Sadhna Arun MALUSARE<sup>1</sup>, Ragini Kundan Prashant AHIWALE<sup>1</sup>, Purnima PATIL<sup>1</sup>, Ayoub GROULI<sup>2</sup>, Mohammed BERRADA<sup>2</sup>, Vikram Rama Uttam PANDIT<sup>1\*</sup>

<sup>1</sup> Department of Chemistry, Haribhai V. Desai College, Pune-411002, India

<sup>2</sup> Department of Chemistry, University Hassan II of Casablanca, Morocco

Corresponding author email\* [vikramupandit@gmail.com](mailto:vikramupandit@gmail.com)

Received: 8 May 2022; Accepted: 8 June; Published: 21 July 2022

## Abstract

*Metal oxide based semiconductor photocatalysts are well known for multifunctional applications. Herein, we have reported the ex-situ synthesis of Fe<sub>2</sub>O<sub>3</sub>-SnO<sub>2</sub> nanocomposite system using simple wet impregnation method. Total five semiconductor nanomaterial photocatalysts were prepared as Fe<sub>2</sub>O<sub>3</sub>, SnO<sub>2</sub>, 1, 2.5 and 5% of SnO<sub>2</sub> over Fe<sub>2</sub>O<sub>3</sub> surface. After successful synthesis of these photocatalysts its formation is checked using UV-Vis spectroscopy, FTIR and RAMAN analysis. Photocatalytic dye degradation performance is checked towards safranin dye using all the five photocatalyst systems. Resultant composite photocatalysts were not showed some impressive photocatalytic activities as compared to individuals. This above observation is may be due to the less gap between conduction band levels of both photocatalyst systems.*

**Keywords:** Composite, Dyes, Degradation, Photocatalysis.

## I. Introduction

Nanostructured semiconductor materials are at the center of attraction among the scientific community due to their fascinating properties like suitable band gap, higher surface area and optical properties [1]. Depending on these impressive properties they are used for extensive range of applications in various fields such as photocatalysis, sensors (gas, humidity), solar cells, optoelectronic and nano devices etc [2]. Particularly, TiO<sub>2</sub>, ZnO, SnO<sub>2</sub>, ZrO<sub>2</sub> and Fe<sub>2</sub>O<sub>3</sub> nanosystems are used as a catalyst for the elimination of organic pollutants. Many complex organic pollutants when released in water sources they remained there for long period of time causing serious ill effects to aquatic life. Mainly, colored complex dyes are playing a very vital role in the water pollution since they are persistent over a long period of time ultimately, that affects the human health [2]. There exist many physical, chemical and biological treatment methods to eliminate this harmful organic dyes.

Photocatalysis is one of the very promising method as it is with very less side products and less cost in comparison to other. TiO<sub>2</sub> is most important and discussed photocatalytic material known till date [3]. Fe<sub>2</sub>O<sub>3</sub> is a semiconducting inorganic material which is also known as Hematite or Red iron oxide which is a promising candidate in photocatalysis. Various other sulfides and oxides are used for making composites with Fe<sub>2</sub>O<sub>3</sub>. On the other hand, SnO<sub>2</sub> is also one of the best semiconducting oxide material which is mostly used for sensing, resistors, optoelectronic devices and photocatalytic applications [4].

In the present article, we have demonstrated the synthesis, characterization and photocatalytic activity of Fe<sub>2</sub>O<sub>3</sub>-SnO<sub>2</sub> nanocomposite. After successful synthesis of these photocatalysts its formation is checked using UV-Vis spectroscopy, FTIR and RAMAN analysis. Photocatalytic dye

degradation performance is checked towards safranin dye using all the five photocatalyst systems [5-7]. Resultant composite photocatalysts were not showed some impressive photocatalytic activities as compared to individuals [8]. This above observation is may be due to the less gap between conduction band levels of both photocatalyst systems [9-11]. These type of nanocomposites may be useful for the removal of other organic complex dyes [12-14].

## II. Experimental

### II.1. Materials

Fe<sub>2</sub>O<sub>3</sub> and SnO<sub>2</sub> nanomaterial used are as it is without any further purification ordered from LOBA chemicals.

#### II.1.1. Synthesis of nanocomposite photocatalyst systems

For the formation of Fe<sub>2</sub>O<sub>3</sub>-SnO<sub>2</sub> nanocomposite systems simple wet impregnation method was employed, which is discussed as below. Both the individual's catalysts were synthesized separately and used after all characterization. Take 0.5gm of Fe<sub>2</sub>O<sub>3</sub> in three different beakers and add 25 mL of ethanol to each with continuous stirring. After 30 min. 1, 2.5 and 5 weight percent of SnO<sub>2</sub> is added with respect to Fe<sub>2</sub>O<sub>3</sub> while continuous stirring. These solutions were kept under constant stirring till the ethanol evaporates completely. Lastly, the powdered composites were heated at 80 °C for 12 hours to get complete dry photocatalyst systems. Before subjected to the XRD, FTIR and Raman spectroscopy characterization these all photocatalytic systems were well mixed using mortar and pestle.

#### II.1.2. Characterizations:

The formation of composite systems with the individuals are checked by using powder XRD (PXRD) technique (20° to 80° range, scan rate = 1° /min) equipped with a monochromator and

Ni-filtered Cu K $\alpha$  radiation from Bruker AXS model D-8. UV-1800, Shimadzu is used for the recording the absorbance value of dye remained solution after each reading. For the molecular identification Raman spectroscopy is used (RENISHAW inVia Raman microscope). For the identification of vibrational modes present in Fe-O and Sn-O bonds FTIR (Shimadzu, IR Affinity-1) is used.

### II.1.3. Photocatalytic dye degradation study

The photocatalytic dye degradation using all the five nanocomposite systems were performed under natural sunlight using following procedure. Herein, we used Safranin dye for the first time. A 10 ppm stock solution (01 liter) of safranin dye was prepared by dissolving 10 mg of dye in 1000 mL DI water. During each degradation experiment 100 ml, 10 ppm of Safranin solutions were taken in 150 mL flask. To this solution 10 mg of photocatalyst systems were added and stirred for 30 min in dark to attend the adsorption desorption equilibrium for the solar light [15-16].

### II.1.4. Photocatalytic degradation of safranin in Sunlight

On the roof top of building a safranin dye solution in a photoreactor were stirred and after fix interval of time 2 mL of samples were removed and centrifuged for 15 min at 3600-3800 rpm to separate the photocatalyst. The supernatant liquid was analyzed using UV-visible spectrophotometer (UV-1800, Shimadzu) to record the change of Safranin concentration. The absorbance value at wavelength 520 nm was used to find out the % dye degradation. The % dye degradation was calculated using equation (1).

$$\% \text{ dye degrade} = (C_0 - C_t) / C_0 \times 100 \dots (1)$$

where,  $C_0$  is an initial concentration of Safranin dye and  $C_t$  is the concentration of Safranin after irradiation time 't'.

## III. Results and Discussions

### III.1. FTIR Analysis

After complete synthesis of Fe<sub>2</sub>O<sub>3</sub>-SnO<sub>2</sub> nanocomposite systems the structural characterization was performed using FTIR analysis.

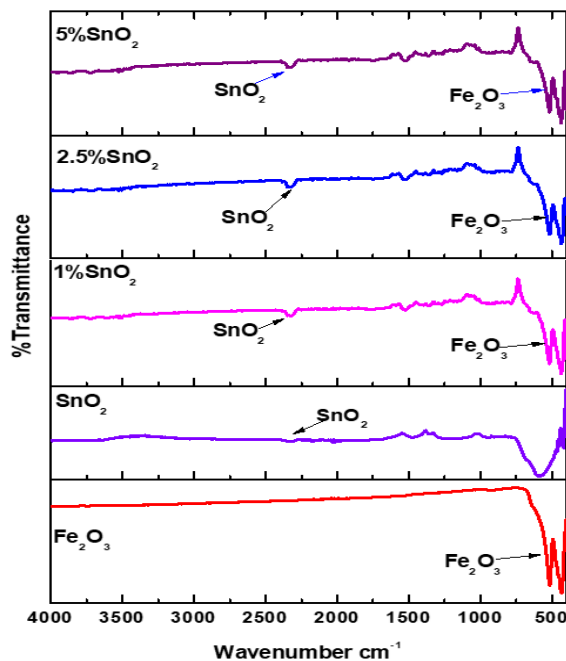


Figure 1: FTIR analysis of Fe<sub>2</sub>O<sub>3</sub>-SnO<sub>2</sub> nanocomposites

Figure 1 shows the FTIR spectrum of Fe<sub>2</sub>O<sub>3</sub>, SnO<sub>2</sub>, 1, 2.5 & 5% Fe<sub>2</sub>O<sub>3</sub>-SnO<sub>2</sub> nanocomposites. From figure it is very clear that the peaks around 450 to 550 cm<sup>-1</sup> are attributed to Fe<sub>2</sub>O<sub>3</sub> nanostructures and no any other prominent peaks were seen in the Fe<sub>2</sub>O<sub>3</sub> spectrum. The peak responsible for SnO<sub>2</sub> vibration were seen at around 550 to 650 cm<sup>-1</sup> the peak at around 2200 to 2250 cm<sup>-1</sup> is due to the SnO<sub>2</sub> nanoparticles. Also, in figure, 1, 2.5 & 5% Fe<sub>2</sub>O<sub>3</sub>-SnO<sub>2</sub> nanocomposites both the peaks of Fe<sub>2</sub>O<sub>3</sub> and SnO<sub>2</sub> were seen which conforms the formation of nanocomposite of SnO<sub>2</sub> over the surface of Fe<sub>2</sub>O<sub>3</sub> nanoparticles [17].

### III.2. X-ray diffraction analysis

Figure 2 depicts the powdered XRD patterns of Fe<sub>2</sub>O<sub>3</sub>, SnO<sub>2</sub>, 1, 2.5 and 5% of Fe<sub>2</sub>O<sub>3</sub>-SnO<sub>2</sub> nanocomposites.

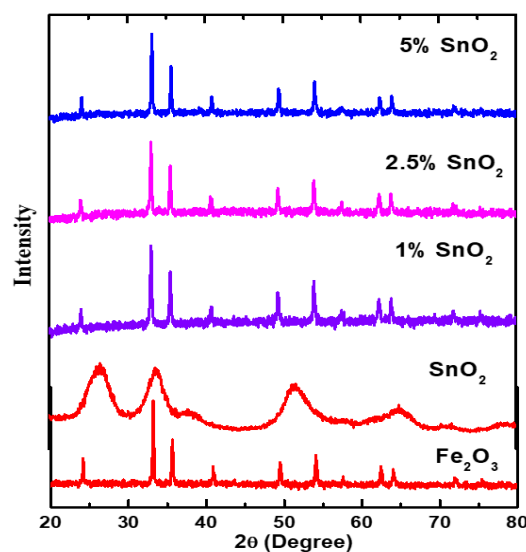


Figure 2. Powdered XRD of Fe<sub>2</sub>O<sub>3</sub>-SnO<sub>2</sub> nanocomposites



From figure it is very clear that  $\text{Fe}_2\text{O}_3$  and  $\text{SnO}_2$  showed resemblance with earlier reports. In 1, 2.5 & 5% of  $\text{Fe}_2\text{O}_3$ - $\text{SnO}_2$  nanocomposites all the peaks attribute to only  $\text{Fe}_2\text{O}_3$  nanostructure and no any prominent peaks for  $\text{SnO}_2$  were seen this might be due to the very less percentage of  $\text{SnO}_2$  used formation on nanocomposite hence not detected in the XRD analysis [18].

### III.3. RAMAN analysis

Raman spectrum of  $\text{Fe}_2\text{O}_3$ - $\text{SnO}_2$  nanocomposites were shown in figure 3. The Raman shift at around  $1300\text{ cm}^{-1}$  is attributed to the  $\text{Fe}_2\text{O}_3$  nanostructure and the spectrum for 1, 2.5 & 5% are fore the  $\text{Fe}_2\text{O}_3$ - $\text{SnO}_2$  nanocomposite. From figure it is very clear that, the peak at around  $650\text{ cm}^{-1}$  is because of  $\text{SnO}_2$  nanoparticles (marked using \* in the diagram). As the concentration of  $\text{SnO}_2$  is increasing over the surface of  $\text{Fe}_2\text{O}_3$  nanoparticle the intensity of  $\text{SnO}_2$  peak is also increases as shown in the Figure [19]. For more clarification, the  $\text{SnO}_2$  peak is highlighted in zoom.

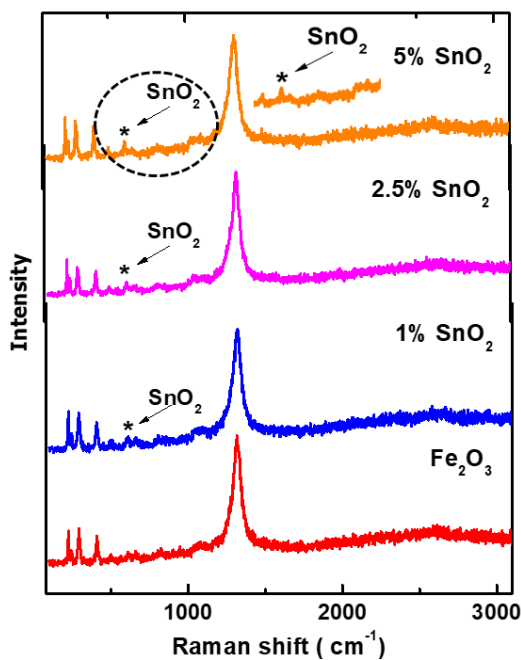


Figure 3. Raman analysis of  $\text{Fe}_2\text{O}_3$ - $\text{SnO}_2$  nanocomposites

### III.4. Photocatalytic Safranin dye degradation

Photocatalytic activity of  $\text{Fe}_2\text{O}_3$ ,  $\text{SnO}_2$  and 1, 2.5 and 5% of  $\text{Fe}_2\text{O}_3$ - $\text{SnO}_2$  nanocomposites were checked in absence of light, without any of the above catalyst and also in presence of all five catalysts. The graph of absorbance studies for all the five photocatalytic systems were showed in figure 4.

From Figure 4 it can be seen that as the time passes the absorbance intensity decreases with different rates depending on the photocatalysts.

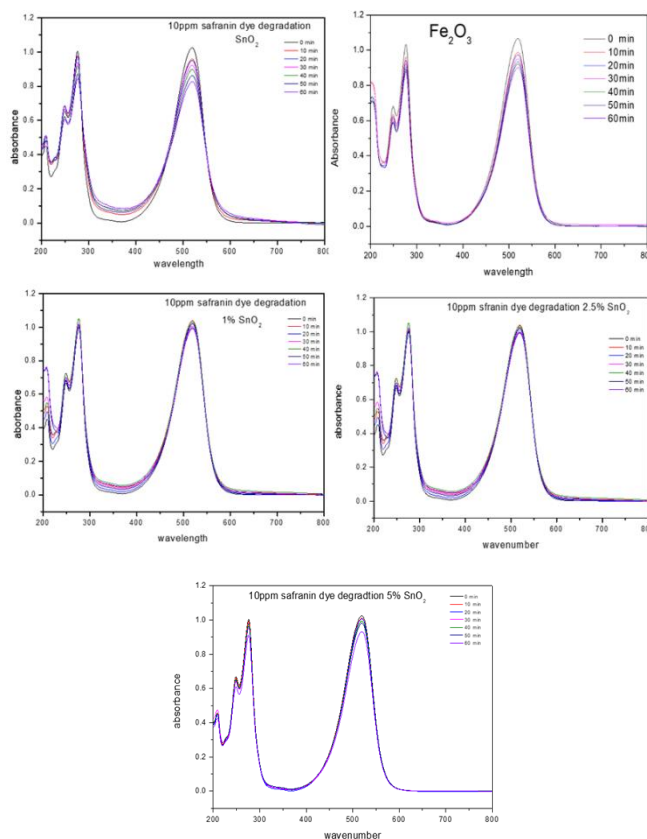


Figure 4: Absorbance graphs of  $\text{Fe}_2\text{O}_3$ ,  $\text{SnO}_2$  1, 2.5 and 5% of  $\text{SnO}_2$  over  $\text{Fe}_2\text{O}_3$  nanocomposite

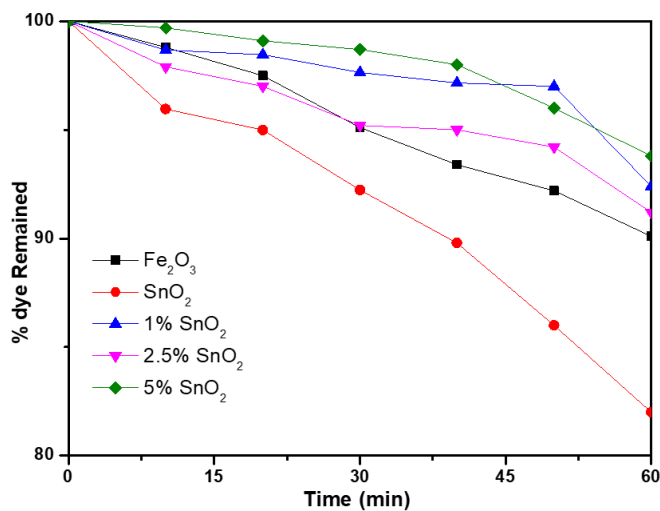


Figure 5. Percent Safranin dye degradation

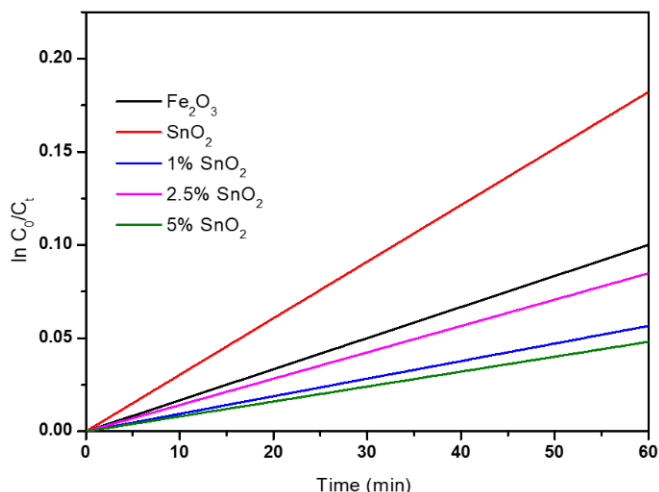


Figure 6. Rate of Safranin dye degradation

Depending on these absorbance graphs, we also calculated and plotted the percentage of Safranin dye degradation as functions of irradiation of 60 time as shown in the figure 5.

All these experiments were done in presence of natural sunlight around 12 noon to 1 PM in day light in order to get maximum light intensity. For Fe<sub>2</sub>O<sub>3</sub> and SnO<sub>2</sub> around 10% and 18% of dye degraded respectively. As the concentration of SnO<sub>2</sub> is increases the rate of degradation was expected to increase, but surprisingly we have not seen any improvement in the rate of degradation. Along with this we also explored the Safranin dye degradation experiments without light (in the dark) and without any of the above photocatalyst semiconductor catalyst. In the dark no Safranin dye degradation found which supports the mechanism of photocatalytic experiments [20-21]. Figure 6 gives the idea about rates of Safranin dye degradation against the time. For the 1, 2.5 and 5% of the SnO<sub>2</sub> over the surface of Fe<sub>2</sub>O<sub>3</sub> rates are almost same. This proves that the 1 to 5% weight is might not be sufficient for the enhancement of activity.

## Conclusions

Ex-situ synthesis of Fe<sub>2</sub>O<sub>3</sub>-SnO<sub>2</sub> nanocomposite system using simple wet impregnation method is reported. All five photocatalysts systems were prepared as Fe<sub>2</sub>O<sub>3</sub>, SnO<sub>2</sub>, 1, 2.5 and 5% of SnO<sub>2</sub> over Fe<sub>2</sub>O<sub>3</sub> surface. After successful synthesis of these photocatalysts its formation is checked using UV-Vis spectroscopy, FTIR and RAMAN analysis. Photocatalytic dye degradation performance is checked towards safranin dye using all the five photocatalyst systems. This above observation is may be due to the less gap between conduction band levels of both photocatalyst systems. Resultant composite photocatalysts were not showed some impressive photocatalytic activities as compared to individuals. These types of hybrid nanosystems can also be utilized for the number of applications.

## Acknowledgement

All the authors thanks to PGK Mandal and Principal of Haribhai V. Desai College, Pune for lab facilities and continuous support.

**Conflict of Interest.** There is no any conflict of interest.

## References

- [1] A. A. Ali, I.S. Ahmed, E.M. Elfiky. Auto-combustion Synthesis and Characterization of Iron Oxide Nanoparticles ( $\alpha$ -Fe<sub>2</sub>O<sub>3</sub>) for Removal of Lead Ions from Aqueous Solution. Journal of inorganic and oragametallic polymers. 31, 384–396, 2021.
- [2] V. V. Pham, M. Cao, V. Le. Insight into the photocatalytic mechanism of tin dioxide/polyaniline nanocomposites for NO degradation under solar light. Journal of Nanomaterials, 2016, 1-8, 2016.
- [3] D. Zhao., W. Xiang. Nanoparticles assembled SnO<sub>2</sub> nanosheet photocatalysts for wastewater purification. Materials Letters, 210, 354-357, 2018.
- [4] R. Mithun Prakash, C. Ningaraju, K. Gayathri, Y.N. Teja, M. Aslam Manthrammel, Mohd. Shkir, S. AlFaify, M. Sakar, One-step solution auto-combustion process for the rapid synthesis of crystalline phase iron oxide nanoparticles with improved magnetic and photocatalytic properties. Advanced Powder Technology, 33, 0921-8831, 2022.
- [5] S. Pandit, S. Bhalerao, U. Aher, G. Adhav, V. Pandit, Amberlyst A-15: Reusable catalyst for the synthesis of 2, 4, 5-trisubstituted and 1, 2, 4, 5-tetrasubstituted-1H-imidazoles under MW irradiation. Journal of Chemical Science. 123, 421-426, 2011.
- [6] G. Kumbhar, V. Pandit, S. Deshmukh, J. Ambekar, S. Arbuj, S. Rane. Synthesis of hierarchical zno nanostructure and its photocatalytic performance study . Journal of Nanoengineering and Nanomanufacturing. 3, 227-231, 2015.
- [7] V. Pandit, S. Arbuj, Y. Pandit, S. Naik, S. Rane, U. Mulik, S. Gosavi, B. Kale. Solar Light driven Dye Degradation using novel Organo-Inorganic (6, 13-Pentacenequinone-TiO<sub>2</sub>) Nanocomposite. RSC Advance. 5, 10326- 1033, 2015.
- [8] V. Pandit, S. Arbuj, U. Mulik, B. Kale. Novel functionality of organic 6, 13-pentacenequinone as a photocatalyst for hydrogen production under solar light. Environmental Science & Technology. 7, 4178-4183, 2014.
- [9] V. U. Pandit, S. S. Arbuj, R. R. Hawaldar, P. V. Kshirsagar, J. D. Ambekar, U. P. Mulik, S. W. Gosavi, B. B. Kale. Hierarchical CdS nanostructure by Lawesson's reagent and its enhanced photocatalytic hydrogen production .RSC advances. 5, 13715-13721, 2015.
- [10] L. Klaai, D. Hammiche, A. Boukerrou, V. Pandit. Thermal and structural analyses of extracted cellulose from olive husk. Materials Today: Proceedings, (2021) <https://doi.org/10.1016/j.matpr.2021.10>.
- [11] A.S. Somwanshi, S.S. Pandit, R.D. Ghogare, V. Pandit, and A.D. Gholap. Effecient catalyst for Knoevenagel condensattion of Aryl Aldehydes with Meldrum's Acid. International journal of Chemistry Physics Science, 7, 92, 2018.

[12] V. Pandit, S. Arbuji, R. Hawaldar, P. Kshirsagar, U. Mulik, S. Gosavi, C. Park, B. Kale. In situ preparation of a novel organo-inorganic 6, 13-pentacenequinone-TiO<sub>2</sub> coupled semiconductor nanosystem: a new visible light active photocatalyst for hydrogen generation. *Journal of Material Chemistry*, 3, 4338-4344, 2015.

[13] V. Jawale, G. Gugale, M. Chaskar, S. Pandit, R. Pawar, S. Suryawanshi, V. Pandit, G. Umarji, S. Arbuji. Two-and three-dimensional zinc oxide nanostructures and its photocatalytic dye degradation performance study. *Journal of Material research*. 36, 1573-1583, 2021.

[14] K. A. Nevase, S. S. Arbuji, V. U. Pandit, J. D Ambekar, S. B. Rane. Synthesis, characterization and photocatalytic activity of tungsten oxide nanostructures. *Journal of Nanoengineering and Nanomanufacturing*. 5, 221-226, 2015.

[15] V. Jawale, A. Al-fahdawi, S. Pandit, G. Dawange, G. Gugale, M. Chaskar, D. Hammiche, S. Arbuji, V. Pandit. 6, 13-pentacenequinone/zinc oxide nanocomposites for organic dye degradation. *Materials Today: Proceedings*. (2021) <https://doi.org/10.1016/j.matpr.2021.10.098>.

[16] S. Pandit, R. Shaikh, V. Pandit . Synthesis of 5-unsubstituted-3, 4-dihydropyridine-2-(1h)-ones using nbs as a catalyst under solvent free conditions. *Rasayan Journal of Organic* . 4, 907-911, 2009.

[17] Dhanesh Gawari, Vikram Pandit, Niteen Jawale, Pramod Kamble. Layered MoS<sub>2</sub> for photocatalytic dye degradation. *Materials Today: Proceedings*, 53, 10-14, 2022.

[18] Shrikant Barkade, Sunil Sable, Varsha Ashtekar, Vikram Pandit. Removal of lead and copper from wastewater using Bael fruit shell as an adsorbent. *Materials Today: Proceedings*, 53, 65-70, 2022.

[19] Pradeep Kate, Vikram Pandit, Vivekanand Jawale, Madhusudan Bachute. L-Proline catalyzed one-pot three-component synthesis and evaluation for biological activities of tetrahydrobenzo [b] pyran: evaluation by green chemistry metrics. *Journal of Chemical Sciences*, 134, 1-11, 2022.

[20] Vikram Pandit. Synthesis of metal sulfides using Lawesson's reagent for photocatalytic hydrogen production. *Materials Today: Proceedings*, 53, 6-9, 2022.

[21] Vikram Pandit. Hydrogen as a Clean Energy Source .*Energy Efficiency*, IntechOpen, (2021) DOI: 10.5772/intechopen.101536.

# Nano-Encapsulation Systems Improve Drug Delivery and Solubility

Lamia TAOUZINET<sup>\*1,2,3</sup>, Sofiane FATMI<sup>2,3,4</sup>, Malika LAHIANI-SKIBA<sup>4</sup>, Mohamed SKIBA<sup>4</sup>, Mokrane IGUER-OUADA<sup>2</sup>

<sup>1</sup>Centre de Recherche en Technologies Agro-Alimentaires (CRTAA), Campus universitaire Tergua Ouzemour, Bejaia.06000. ALGERIA

<sup>2</sup>Associated Laboratory in Marine Ecosystems and Aquaculture, Faculty of Nature and Life Sciences, University of Bejaia, 06000 Bejaia, Algeria

<sup>3</sup>Technology Pharmaceutical Laboratory, Department of Processes Engineering, Faculty of Technology, Université de Bejaia, 06000 Bejaia, Algeria.

<sup>4</sup>Technology Pharmaceutical and Bio Pharmaceutics Laboratory, UFR Medicine and Pharmacy, Rouen University, 22 Blvd. Gambetta, 76183, Rouen, France.

\* Corresponding Author: TAOUZINET Lamia E-mail: [lamia.taouzinet@crtaa.univ-bejaia.dz](mailto:lamia.taouzinet@crtaa.univ-bejaia.dz)

Received: 05 May 2022; Accepted: 05 June 2022; Published: 20 July 2022

## Abstract

*Size reduction is one of the most often utilized and important unit processes in pharmaceutical manufacture. It contributes to increased medicine safety and bioavailability, decreased toxicity, improved drug release, and improved drug formulation possibilities. Nanoencapsulation is a process that involves encapsulating a bioactive molecule in liquid, solid, or gaseous form within a matrix of inert material in order to preserve the coated component. The size of nanoencapsules can range from 1 to 1,000 nm. They have a multitude of different shapes, depending on the materials and methods used to prepare them. The main reason for nanoencapsulation species is to ensure that the encapsulated material reaches the area of action without being adversely affected by the external environment through which it passes. This research concentrated on current breakthroughs in nanoencapsulation drug systems, production, and characterization methodologies.*

**Keywords** Nanoencapsulation, Drug delivery, Solubility.

## I. Introduction

Nanotechnology can enable improved medication delivery methods for better disease management and treatment by manipulating the properties of materials like polymers and fabricating nanostructures.

The most important application of clinical nanotechnology, it is predicted, will be in pharmaceutical development within a short period of time [1]. From the micro to the nanoscale, drug delivery research is now progressing. Novel approaches for controlled release, targeted delivery, and enhanced bioavailability have been associated with the technology of nanoparticles (NPs) as drugs or constituents of drugs [2]. Polymer capsules made at the nanoscale provide advantages such as drug breakdown, controlled drug release, and excellent absorption at the target location [3]. Scientists across the world are now working to develop novel polymers, refine existing ones, and test particular polymer-drug combinations. Nanocapsules, for example, have been made from monomers or by simple nano deposition of a polymer that has been accomplished [4]. Through diagnostic and therapeutic agent transportation, nanomaterials are formulated in a unique way to make contact with molecules, interact with them, and detect any changes at the molecular level [1, 5]. Fabrication of nanoscale materials and devices can be done from the bottom up or from the top down. Bottom-up methods fabricate nanomaterials or structures from a controlled buildup of atoms or molecules, which is regulated by thermodynamic means such as self-assembly [6]. Microtechnologies, on the other

hand, can be used to fabricate nanoscale structures and devices. Photolithography, nanomolding, dip-pen lithography, and nanofluids are examples of top-down nanofabrication technologies [7]. As a result, advancements in this field will lead to improved drug delivery, as well as other applications in medicine and pharmacy, as well as methods of preparation.

## II. Nanotechnology-based drug delivery systems

Several nanoparticles and nanomaterials have been studied and authorized for usage in therapeutic settings. The following sections go over some of the most prevalent forms of nanoparticles.

**Micelles:** Micelles are lipid- and amphiphilic-molecule-based amphiphilic surfactant molecules. Micelles spontaneously aggregate and self-assemble into spherical vesicles with a hydrophilic outer monolayer and a hydrophobic core in aqueous circumstances, allowing hydrophobic medicinal substances to be included. Micelles' unique characteristics allow for increased solubility of hydrophobic medicines, resulting in improved bioavailability. Micelles have a diameter of 10 to 100 nm. Micelles are used as drug delivery agents, imaging agents, contrast agents, and therapeutic agents, among other things [8].

**Liposomes:** Liposomes are vesicular structures made up of one or more lipid bilayers and an equal number of aqueous compartments [9]. Liposomes range in size from the tiniest vesicle (diameter 20nm) to liposomes with a diameter of 1m

or larger, about comparable to the dimensions of live cells, and may be observed under a light microscope. One or three compartments in a liposome can carry medicines (water soluble agents in the central aqueous core, lipid soluble agents in the membrane, peptide and small proteins at the lipid aqueous interface) [10]. Phospholipids, which are molecules with a head group and a tail group, are commonly used to make membranes. The head is attracted to water, whereas the tail, which is made up of a long hydrocarbon chain, is repelled by it. A liposome is a self-forming structure made up of one or more concentric lipid bilayers separated by water buffer compartments and is a lipid bilayer-based artificially produced spherical vesicle [11].

**Dendrimers:** Dendrimers are a new type of polymer with a controlled structure and nanometric dimensions. Dendrimers, which are utilized in drug administration and imaging, are typically 10 to 100 nm in diameter and have numerous functional groups on their surface, making them suitable drug carriers [12]. Dendrimers have been extensively researched in terms of their structure and function. Dendrimers nowadays can be extremely specialized, encasing functional molecules [therapeutic or diagnostic agents) within their core [13]. They can be manufactured into metallic nanostructures and nanotubes, as well as having an encapsulating capability, and they are compatible with organic structures such as DNA. Dendrimers are used extensively in the medical and biological areas because they have various reactive surface groups [nanostructure) and are compatible with organic structures such as DNA. Nonsteroidal anti-inflammatory formulations, antibacterial and antiviral medicines, anticancer agents, pro-drugs, and screening agents for high-throughput drug discovery are among the medicinal applications of dendrimers [14] Because of their propensity to break cell membranes due to a positive charge on their surface, dendrimers may be hazardous [15].

**Carbon nanotubes:** Carbon nanotubes are cylinders made up of single-layer carbon atoms wrapped together into sheets [graphene). They can be single walled, multi walled, or made up of several concentrically interconnected nanotubes [16]. Carbon nanotubes can reach extremely high loading capacities as drug carriers due to their large exterior surface area. Carbon tubes are also useful as imaging contrast agents [17] and biological sensors due to their unique optical, mechanical, and electrical characteristics [18].

**Metallic nanoparticles:** Iron oxide and gold nanoparticles are examples of metallic nanoparticles. A magnetic core (45 nm) and hydrophilic polymers, such as dextran or PEG [16], make up iron oxide nanoparticles. Gold nanoparticles, on the other hand, have a gold atom core surrounded by negative reactive groups on the surface, which may be functionalized by adding a monolayer of surface moieties as ligands for active targeting [18]. Metallic nanoparticles have been used as imaging contrast agents [19], in laser-based treatment, as optical biosensors and drug delivery vehicles [20].

**Quantum dots:** Quantum dots (QDs) are fluorescent semiconductor nanocrystals with a diameter of 1100 nm that have showed promise in a variety of biological applications, including medication delivery and cellular imaging [21]. Quantum dots have a shellcode structure, which is generally made up of elements from the II-VI or III-V groups of the periodic table. Quantum dots have been used in medical imaging because of their unusual optical characteristics and size, as well as their great brightness and stability [21].

### III. Preparation methods

#### *High-pressure homogenization technique*

On a big scale, this method is employed. It can be done in one of two ways: cold homogenization or hot homogenization. Stress is given to the lipid by applying high pressure through extremely high shear, and it is pushed through a specially constructed homogenization valve to produce suspended particles with a homogeneous size distribution. It's crucial to understand that, depending on the nature of the medication and excipients, both raised and below room temperature can be utilized [22].

#### *Supercritical Fluid Technology*

Supercritical fluids are non-hazardous to the environment. Supercritical antisolvent (SAS), rapid expansion of supercritical solution (RESS), and precipitation with compressed antisolvent process (PCS) are all typical supercritical fluids techniques. Two fully miscible solvents are used in the SAS technique: one is supercritical liquid and the other is a fluid solvent. While the solutes are insoluble in supercritical liquid, nanoparticulates are generated as a result of the rapid precipitation of solutes formed as a result of the supercritical fluid's extraction of the fluid solvent. The solutes are dissolved into the supercritical liquid in the RESS method, which results in a considerable loss of solvent power and therefore precipitation of the solutes owing to fast extension of solutes through tiny nozzle into the area of reduced pressure. Meziani et al. (2004) used a supercritical fluid method to make nanoparticles of Poly (heptadecafluorodecyl acrylate) with a diameter of >50nm. Although organic solvents are not required in the RESS approach for nanoparticle production, the main disadvantage is that the products formed at the primary step are microscaled rather than nanoscaled. However, a newer supercritical fluid technique known as RESOLV is presently in use, in which a fluid solvent inhibits particle development in the expansion jet nozzle, resulting in the creation of nanoscaled particulates in their early stages [23].

#### *Emulsion-Solvent Evaporation Method*

One of the most common ways for preparing nanoparticles is this approach. There are two processes to emulsification-solvent evaporation. The polymer solution must first be emulsified into an aqueous phase in the first stage.

The polymer solvent is evaporated in the second stage, causing the polymer to precipitate as nanospheres. The nano particles are collected by ultracentrifugation and then washed

with distilled water to eliminate any remaining stabilizers or free drugs before being lyophilized for storage). The highpressure emulsification and solvent evaporation technique is a variation of this process . This process begins with the creation of an emulsion, which is then homogenized under high pressure before being stirred to remove the organic solvent. The size may be adjusted by altering the stirring rate, dispersion agent type and quantity, organic and aqueous phase viscosity, and temperature . This method, on the other hand, can be used to make liposoluble drugs, with the scale-up issue posing a limitation [24].

#### ***Solvent Displacement / Precipitation Method***

In the presence or absence of surfactant, solvent displacement entails the precipitation of a preformed polymer from an organic solution and the diffusion of the organic solvent into the aqueous medium. In a semipolar water miscible solvent like acetone or ethanol, polymers, drugs, and/or lipophilic surfactants are dissolved. Under magnetic stirring, the solution is emptied or injected into an aqueous solution containing stabilizer. Rapid solvent diffusion produces nanoparticles very instantly [24].

#### ***Double Emulsion and Evaporation Method***

To encapsulate hydrophilic medicines, the double emulsion approach is used, which includes adding aqueous drug solutions to organic polymer solutions while vigorously swirling to produce w/o emulsions. This w/o emulsion is continuously stirred into the second aqueous phase to create the w/o/w emulsion. The emulsion is subsequently evaporated to remove the solvent, and nano particles may be separated using high-speed centrifugation. Before lyophilization, the formed nanoparticles must be thoroughly washed [25]. The amount of hydrophilic drug to be integrated, the stabilizer concentration, the polymer concentration, and the volume of the aqueous phase are the factors that influence nano particle characterisation in this approach [26].

#### **IV. Different advantages of nano sized drug delivery system over conventional dosage forms**

In comparison to conventional dosage forms or drug delivery techniques, we got the following benefits using nanotechnology [27, 28]:

- Higher bioavailability for drugs having low solubility.
- Nanotechnology offers a wide range of applications (I.V, Oral, dermal etc.)
- There is a well-established method of preparation for large-scale manufacturing, namely high-pressure homogenization.
- Improved bioavailability, sustained and controlled release characteristics, and environmental hazard protection for medicinal molecules.
- Vaccines, anticancer drugs, and other biological products are good candidates for delivery.
- Nanotechnology might be used to conduct tissue editing on a nan size.

#### **V. Characterization of Nanoparticles**

*Particle size:* The most significant factors in nanoparticle characterisation are particle size distribution and shape. Electron microscopy is used to determine morphology and size. Nanoparticles are most commonly used in medication delivery and targeting. It has been discovered that particle size has an impact on medication release. The surface area of smaller particles is greater. As a result, the majority of the drug placed onto them will come into contact with the particle surface, resulting in rapid drug release. Drugs, on the other hand, slowly diffuse inside bigger particles. Smaller particles tend to agglomerate during storage and transit of nanoparticle dispersion, which is a disadvantage. As a result, there is a compromise between nanoparticle size and optimum stability [29]. The particle size has an impact on polymer degradation. In vitro, for example, the breakdown rate of poly (lactic-co-glycolic acid) increased with increasing particle size [30]. As mentioned below, there are many techniques for measuring nanoparticle size.

Dynamic light scattering (DLS),  
Scanning electron microscopy (SEM)  
Transmission electron microscope (TEM)  
Atomic force microscopy (AFM)

*Surface Charge:* The type and strength of a nanoparticle's surface charge is critical since it influences how it interacts with the biological environment as well as how it interacts electrostatically with bioactive substances. The zeta potential of nanoparticles is used to assess colloidal stability. This potential is a proxy for the charge on the surface. It is the difference in potential between the outer Helmholtz plane and the shear surface. The measurement of the zeta potential allows for predictions about the storage stability of colloidal dispersion. High zeta potential values, either positive or negative, should be achieved in order to ensure stability and avoid aggregation of the particles. The zeta potential measurements can then be used to determine the amount of surface hydrophobicity. The nature of the substance contained within the nanocapsules or coated onto the surface may also be determined using the zeta potential [31].

*Surface hydrophobicity:* Several methods, such as hydrophobic interaction chromatography, biphasic partitioning, probe adsorption, and contact angle measurements, can be used to evaluate surface hydrophobicity. Several advanced analytical methods for surface examination of nanoparticles have recently been published in the literature. The detection of particular chemical groups on the surface of nanoparticles is possible using X-ray photon correlation spectroscopy [32].

*Drug Release:* Understanding the way and amount to which drug molecules are released is essential since one of the main reasons for studying nanotechnology is to deliver medicines. Most release techniques need the separation of the medication and its delivery vehicle in order to get this information. The

quantity of drug bound per mass of polymer (typically moles of drug per mg polymer or mg drug per mg polymer) is referred to as nanoparticle drug loading. It can also be expressed as a percentage of the polymer. Classic analytical techniques such as UV spectroscopy or high-performance liquid chromatography (HPLC) following ultracentrifugation were employed for this analysis. UV spectroscopy or HPLC are used for quantification. Drug release assays are comparable to drug loading assays, which are used to determine the mechanism of drug release over time [33].

## VI. Application nanotechnology examples

### *Nanotechnology and cancer treatment*

A staggering number of people worldwide are affected by cancer, underlining the need for a more precise diagnosis technique as well as a revolutionary medication delivery system that is more targeted, efficient, and has fewer adverse effects [34]. Anticancer therapies are frequently seen to be preferable if the therapeutic agent is able to reach the precise target spot without causing any adverse effects. The surface of nanoparticle carriers might be chemically modified to facilitate the needed targeted delivery. The inclusion of PEG, or polyethylene oxide, at the surface of nanoparticles is one of the greatest instances of surface modifications. These changes improve not just the selectivity of medication absorption, but also the capacity to target tumors. PEG prevents the body's immune system from recognizing nanoparticles as foreign objects, allowing them to circulate in the bloodstream until they reach the tumor. Hydrogel's use in breast cancer treatment is also an excellent illustration of this cutting-edge technology. Herceptin is a monoclonal antibody that targets the human epidermal growth factor receptor 2 (HER2) on cancer cells in the treatment of breast cancer. With just a single dosage of Herceptin, a vitamin E-based hydrogel has been created that can transport the drug to the target location for several weeks. The hydrogel-based drug delivery is more efficient than traditional subcutaneous and intravenous drug administration modalities because Herceptin is retained better within the tumor, making it a superior anti-tumor agent [35-37]. Through the use of nanotechnologies, nanoparticles may be changed in a variety of ways to extend circulation, improve drug localization, boost therapeutic effectiveness, and perhaps reduce the development of multidrug resistance. Several studies have used FDA-approved nano medicines as adjuvants in combinatory cancer treatment, a nanoparticle formulation of paclitaxel albumin stabilized [nab paclitaxel], has been authorized for the treatment of metastatic breast cancer [38]. According to ClinVar, there are over 900 active clinical studies utilizing nab paclitaxel as an anticancer drug. Furthermore, when utilized in combination with 5 chloro 2.4 dihydroxypyridine, tegafur, and oteracil potassium for the treatment of HER2 negative breast cancer patients, nab paclitaxel showed good outcomes [39].

### *Nanotechnologies for the treatment of cardiovascular diseases*

The properties of nanoparticles can also be used to treat cardiovascular disorders. Cardiovascular illnesses are the main

cause of mortality worldwide, and rates are rising at an alarming rate because of sedentary lifestyles [40]. Stroke, hypertension, and a limitation or blockage of blood circulation in a specific location are common instances of cardiovascular illnesses that affect several people. These illnesses are the leading causes of long-term disability and mortality [40]. Nanotechnologies provide up new therapeutic and diagnostic possibilities for cardiovascular disease treatment. The majority of cardiovascular risk factors (such as hypertension, smoking, hypercholesterolemia, homocystinuria, and diabetes mellitus) are linked to decrease NO endothelium production. The initial stage in the development of atherosclerosis is endothelial dysfunction. NO bioavailability occurs when gold and silica nanoparticles are combined [41]. The 17E loaded CREKA-peptide-modified-nanoemulsion system has been shown to reduce the levels of pathological contributors to early atherosclerosis by reducing lesion size, lowering circulating plasma lipids, and decreasing gene expression of inflammatory markers associated with the disease when administered systemically [42]. Furthermore, innovative formulations of block copolymer micelles made with PEG and poly(propylene sulphide) have been shown to decrease the levels of proinflammatory cytokines [43], indicating that they have great promise for atherosclerosis treatment [43].

For the prevention of platelet aggregation, atherosclerosis, and thrombosis, drug administration through liposomes has been shown to be effective. Vasodilation, platelet aggregation inhibition, leukocyte adhesion, and anti-inflammatory characteristics are all pharmacological features of prostaglandin E1 (PGE1). Liposomal PGE1 medication delivery (Liprostin™) is now in phase III clinical studies for the treatment of a variety of cardiovascular conditions, including restenosis after angioplasty [44]. The use of liposomes encapsulating the thrombolytic drug urokinase has also been investigated; cyclic arginylglycylglycylaspartic acid (cRGD) peptide liposomes encapsulated with urokinase can preferentially attach to the GPIIb/IIIa receptors, improving the thrombolytic effectiveness of urokinase by approximately [44]. Novel nanotherapeutic methods can also improve the efficacy and efficiency of traditional thrombolytic medicines. Drugs can be mechanically activated within blood arteries to specifically target vascular blockage locations based on the high fluid shear stresses existing within them. In vivo and in vitro investigations have been positive, indicating that this method may be used to dissolve blood clots while requiring a considerably lower dose of thrombolytic medication [41-45]. The usage of dendrimers is one example of this technique. Dendrimers have been utilized to deliver medicinal medicines in a variety of illnesses. Plasminogen activator (rtPA) has been effectively linked to dendrimers, resulting in an alternative drug delivery method that allows for precise tuning of the rtPA dendrimer complex concentration over time by varying the dilution proportions of each member of the complex [45]. Another possible use for nanoparticles is to reduce haemorrhaging, which is a common adverse effect of thrombolytic drugs. Targeted thrombolysis using rtPA bound to polyacrylic acid coated nanoparticles reduces intracerebral hemorrhage and improves target site retention [46]. The use of nanotechnologies has helped to reduce medication adverse

effects while also needing lower drug dosages to treat cardiovascular illnesses. Drugs may now be transported to target locations with more carrier capacity, specificity, and stability because to recent advancements in nanotechnology research for drug delivery systems, notably in terms of their water insoluble characteristics. Researchers have been able to design formulations that can enhance medication efficiency while lowering costs because to continuous developments in nanoparticle drug delivery technologies [47].

#### *Nanotechnologies for sperm cryoprotection*

Several nanoparticle compositions with significant antioxidant, anti-inflammatory, and antibacterial activities have been developed as a result of recent developments in nanoparticle technology [7–9]. This certainly offers up a lot of possibilities for improving reproductive functioning in vitro or in vivo [10]. Nanoparticles with antioxidative characteristics may be especially useful for sperm function and male fertility. Semen cooling and cryopreservation have been shown to enhance oxidative stress in spermatozoa, lowering their fertilization ability significantly [11]. After 48 hours and up to 96 hours of incubation, CeO<sub>2</sub> supplementation in the semen extender enhanced motility metrics and boosted sperm cell velocity. Treatment of sperm from several species with cyclodextrins pre-loaded with an appropriate therapeutic molecule [antioxidants, essential oil] before cryopreservation has been shown to enhance sperm quality following the freezing-thawing process. PEGs have a beneficial effect when used in sperm cryopreservation. Treatment of rabbit sperm with vitamin E distributed in PEG 6000 (PEG/Vit E) protected sperm cells after freezing at 4 °C, according to Amokrane et al. (2020) [48]. Recent research has sparked interest in utilizing liposomal formulations as preservation diluents, lowering the danger of egg yolk contamination and raising the value of sperm quality through improved sperm protection [38, 39]. After 48 hours of cooling, the liposome/vitamin E combination also improves motility metrics.

#### **VII. Conclusions**

Nanotechnology has emerged as a critical technique for overcoming drug flaws and enabling medicines to target specific cells or tissues passively or actively. The benefits of nanotechnology systems as drug delivery vehicles in cancer, cardiovascular disorders, and sperm cryoprotection were highlighted in this paper. Future research should concentrate on the effects of therapeutic nanomedicine on performance, molecular mechanisms, and possible toxicity during treatment.

#### *Acknowledgements*

The authors thank the General Directorate of Scientific Research and Technological Development (DGRSDT/MESRS-Algeria) for their financial support.

**Conflict of interest.** The authors report no conflict of interest.

#### **References**

- [1] I. Khan, M. Khan, M.N Umar, D-H. Oh. Nanobiotechnology and its applications in drug delivery system: a review. *IET Nanobiotechnol*, 1-5, 2015.
- [2] J.A. Crommelina Daan , G. Storma, W. Jiskoota, R. Stenekesa, E. Mastrobattista , Wim E. Hennink, Nanotechnological approaches for the delivery of macromolecules. *Journal of Controlled Release*, 87, 81-88, 2003.
- [3] K. Na, Y.H. Bae, Self-Assembled Hydrogel Nanoparticles Responsive to Tumor Extracellular pH from Pullulan Derivative/Sulfonamide Conjugate: Characterization, Aggregation, and Adriamycin Release in Vitro. *Pharmaceutical Research*, 19(5), 681-688, 2002.
- [4] P. couveureur, G. barrat, E. fattal, P. legrand et C. vauthier .Nanocapsule technology: Review. *Critical Reviews in therapeutic drug carrier systems*, 19, 99-134, 2002.
- [5] Y. Xia, Y. Xiong, B. Lim, E. Skrabalak. Shape-Controlled Synthesis of Metal Nanocrystals: Simple Chemistry Meets Complex Physics. *Angewandte Chemie International Edition*, 48, 60-103, 2009.
- [6] M. Ferrari. Cancer nanotechnology: opportunities and challenges. *Nature Reviews Cancer*, 5, 161–171, 2005.
- [7] N.A Peppas. Intelligent therapeutics: biomimetic systems and nanotechnology in drug delivery. *Advanced Drug Delivery Reviews*, 56, 1529-31, 2004.
- [8] T. Matoba. Anti-inflammatory Nanomedicine for Cardiovascular Disease. *Frontiers in Cardiovascular Medicine*, 4, 13, 2017.
- [9] M. Luo, S. Hua, Q. Shang. Application of nanotechnology in drug delivery systems for respiratory diseases (Review). *Molecular medicine reports*, 23, 325, 2021.
- [10] M. Kumar, A. Singh, S. Pandey, M. Siddiqui, N. Kumar. Liposomes: Type, Preparation and Evaluation. *International Journal of Indigenous Herbs and Drugs*, 17-22, 2021.
- [11] B. Alberts, A. Johnson, J. Lewis. *The Lipid Bilayer, Molecular Biology of the Cell*. 4th edition. New York: Garland Science, 2002.
- [13] C. Jin, K. Wang, A. Oppong-Gyebi, J. Hu. Application of Nanotechnology in Cancer Diagnosis and Therapy - A Mini-Review. *International Journal of Medical Sciences*, 17, 2964-2973, 2020.
- [14] X. Chen, D. Yang, Y. Mo, L. Li, Y. Chen, Y. Huang. Prevalence of polycystic ovary syndrome in unselected women from southern China. *European Journal of Obstetrics & Gynecology and Reproductive Biology*, 139, 59-64, 2020.
- [15] R. Mecke, M. Helena, M. Galileo. A review of the weevil fauna [Coleoptera, Curculionoidea] of *Araucaria angustifolia* (Bert.) O. Kuntze [Araucariaceae] in South Brazil. *Revista Brasileira de Zoologia*, 21, 505–513, 2004.
- [16] K. Nune, P. Gunda, P. Thallapally, Y. Lin, M. Laird Forrest, J. Cory. Nanoparticles for biomedical imaging. *Expert Opin Drug Deliv*, 6, 1175–1194, 2009.
- [17] C. Medina, M.J. Santos-Martinez, A. Radomski, OI. Corrigan and MW. Radomski. REVIEW: Nanoparticles: pharmacological and toxicological significance. *British Journal of Pharmacology*, 150, 552-558, 2007.



- [18] J. Bernhol, Christopher Roland, Boris Yakobson. Nanotubes. Current opinion in solid state and materials science, 2 (6), 706-715, 1997.
- [19] S. Acharya, SK. Sahoo. PLGA nanoparticles containing various anticancer agents and tumour delivery by EPR effect. Advanced Drug Delivery Reviews, 63,170-83, 2011.
- [20] WJM. Mulder, GJ. Strijkers, GAF. Van Tilborg, DP. Cormode, ZA. Fayad, K. Nicolay. Nanoparticulate Assemblies of Amphiphiles and Diagnostically Active Materials for Multimodality Imaging. Accounts of Chemical Research, 42, 904-14, 2009.
- [21] CE. Probst, P. Zrazhevskiy, V. Bagalkot, X. Gao. Quantum dots as a platform for nanoparticle drug delivery vehicle design. Advanced Drug Delivery Reviews, 65,703-18, 2013.
- [22] A. ALHaj, R. Abdullah, S. Ibrahim, A. Bustamam. Tamoxifen Drug Loading Solid Lipid Nanoparticles Prepared by Hot High Pressure Homogenization Techniques. American Journal of Pharmaco and Toxicology, 219-224, 2008.
- [23] MJ. Meziani, P. Pathak, R. Hurezeanu, MC. Thies, RM. Enick, Y-P. Sun. Supercritical-Fluid Processing Technique for Nanoscale Polymer Particles. Angewandte Chemie International Edition, 43, 704-7, 2004.
- [24] B. Kamboj, A. Kumar, MS. Hooda, P. Sangwan. Nanotechnology: Various methods used for preparation of Nanomaterials. Asian Journal of Pharmacy and Pharmacology, 4, 356-93, 2018.
- [25] J. Vandervoort, A. Ludwig. Biodegradable stabilizers in the preparation of PLGA nano particles: a factorial design study. International Journal of Pharmaceutics, 238, 77-92, 2002.
- [26] N. Ubrich, P. Bouillot, C. Pellerin, M. Hoffman, P. Maincent. Preparation and characterization of propranolol hydrochloride nano particles: A comparative study. Journal of Controlled Release, 291-300, 2004.
- [27] D. Thassu, M. Deeleers, Y. Pathak. Handbook of Nanoparticulate Drug Delivery System, Informa Healthcare USA, Inc. New York. 166, 6-8, 2007.
- [28] B. Nagavarma, H. Yadav, A. Ayaz, L. Vasudha, S. Kumar. Different techniques for preparation of polymeric nanoparticles. Asian Journal of Pharmaceutical and Clinical Research, 5, 16-20, 2012.
- [29] H M. Redhead, SS. Davis, L. Illum. Drug delivery in poly (lactide-co-glycolide) nanoparticles surface modified with poloxamer 407 and poloxamine 908: in vitro characterisation and in vivo evaluation. Journal of Controlled Release, 70, 353, 2001.
- [30] L. Betancor, HR. Luckarift. Bioinspired enzyme encapsulation for biocatalysis. Trends in Biotechnology, 26, 566, 2008.
- [31] Z. Pangi, A. Beletsi, K. Evangelatos. PEG-ylated nanoparticles for biological and pharmaceutical application. Advanced Drug Delivery Reviews, 24, 403-419, 2003.
- [32] PD. Scholes, AG. Coombes, L. Illum, SS. Davis, JF. Wats, C. Ustariz, M. Vert, MC. Davies. Detection and determination of surface levels of poloxamer and PVA surfactant on biodegradable nanospheres using SSIMS and XPS. Journal of Controlled Release, 59, 261-278, 1999.
- [33] B. Magenhein, M. Levy, S Benita. A new in vitro technique for the evaluation of drug release profile from colloidal carrier ultrafiltration technique at low pressure. International Journal of Pharmaceutics, 94,115-123, 993.
- [34] R. Siegel, D Naishadham, A. Jemal. Cancer statistics. CA: A Cancer Journal for Clinicians, 63, 11-30, 2013.
- [35] LE van Vlerken, TK Vyas, MM Amiji. Polyethylene glycol-modified nanocarriers for tumor-targeted and intracellular delivery. Pharmaceutical Research, 24, 1405-1414, 2007.
- [36] AK. Biswas, R. Islam, ZS. Choudhury, A. Mostafa and MF. Kadir. Nanotechnology based approaches in cancer therapeutics. Advances in Natural Sciences: Nanoscience and Nanotechnology, 5, 2043-6262, 2004.
- [37] P. Gupta, K. Vermani, S. Garg. Hydrogels. From controlled release to pH- responsive drug delivery. Drug Discovery Today, 7, 569-579, 2002.
- [38] AJ. Montero, B. Adams, CM. Diaz-Montero, S. Glück. Nab-Paclitaxel in the treatment of metastatic breast cancer: A comprehensive review. Expert Review of Clinical Pharmacology, 4, 329-334, 2011.
- [39] J. Tsurutani, K. Kuroi, T. Iwasa, M. Miyazaki, S. Nishina, C. Makimura, J. Tanizaki, K. Okamoto, T. Yamashita, T. Aruga. Phase I study of weekly nab-paclitaxel combined with S-1 in patients with human epidermal growth factor receptor type 2-negative metastatic breast cancer. Cancer Science, 106, 734-739, 2015.
- [40] Jr. McGill HC, CA. McMahan and SS. Gidding. Preventing heart disease in the 21st century: Implications of the Pathobiological Determinants of Atherosclerosis in Youth (PDAY) study. Circulation. 117, 1216-1227, 2008.
- [41] A. Das, P. Mukherjee, SK. Singla, P. Guturu, MC. Frost, D. Mukhopadhyay, VH. Shah and CR. Patra. Fabrication and characterization of an inorganic gold and silica nanoparticle mediated drug delivery system for nitric oxide. Nanotechnology, 21, 30510, 2010.
- [42] D. Deshpande, S. Kethireddy, DR. Janero and MM. Amiji. Therapeutic efficacy of an  $\omega$ -3-fatty acid containing 17- $\beta$  estradiol nano-delivery system against experimental atherosclerosis. PLoS One. 11, e0147337, 2016.
- [43] T. Wu , X. Chen , Y. Wang , H. Xiao , Y. Peng , L. Lin , W. Xia , M. Long , J. Tao and X. Shuai. Aortic plaque-targeted andrographolide delivery with oxidation-sensitive micelle effectively treats atherosclerosis via simultaneous ROS capture and anti-inflammation. Nanomedicine. 14, 2215-2226, 2018.
- [44] U. Bulbake, S. Doppalapudi, N. Kommineni, W. Khan. Liposomal formulations in clinical use: An updated review. Pharmaceutics, 9, 12, 2017.
- [45] M. Najlah, S. Freeman, D. Attwood, A. D'Emanuele. In vitro evaluation of dendrimer prodrugs for oral drug delivery. International Journal of Pharmaceutics, 336, 183-190, 2007.

- [46] S. Katsuki, T. Matoba, JI. Koga, K. Nakano, K. Egashira. Anti-inflammatory Nanomedicine for Cardiovascular Disease. *Frontiers in cardiovascular Medicine*, 4, 87, 2017.
- [47] N. Korin, MJ.Gounis, AK. Wakhloo and DE. Ingber. Targeted drug delivery to flow-obstructed blood vessels using mechanically activated nanotherapeutics. *JAMA Neurology*, 72, 119-122, 2015.
- [48] A. Amokrane, R. Kaidi, M. Iguer-Ouada. The effect of vitamin E and poly ethylene glycol (PEG) association on chilled rabbit sperm: impact on sperm motility and oxidative stress status. *CryoLetters*, 41,19-25, 2020.

# Preparation and Characterization of Starch Based Bioplastic Film from Potatoes

Lisa KLAAI\*, Sonia IMZI, Dalila HAMMICHE, Amar BOUKERROU

Laboratoire des Matériaux Polymères Avancés, Département Génie des Procédés, Faculté de Technologie, Université de Bejaia, Algérie.

Corresponding author email\* [lisa.klaai@univ-bejaia.dz](mailto:lisa.klaai@univ-bejaia.dz)

Received: 11 May 2022; Accepted: 11 June; Published: 21 July 2022

## Abstract

*The aim of this study is to develop a bioactive biodegradable film based on starch and glycerol. Starch was extracted from potato. Two films were developed with different concentrations of glycerol (20 and 30%), humidity level, infrared spectroscopy analysis with Fourier transform (FTIR), thermogravimetric analysis and biodegradability test of these films were evaluated. Infrared spectral analysis showed that the 30% and 20% glycerol films have the same chemical structure and no functional group changes occurred. Thermogravimetric analysis showed that a 30% glycerol film has higher thermal stability than a 20% glycerol film. Biodegradability test showed that the lower the percentage of glycerol, the more easily the biofilm degrades.*

**Keywords:** Biodegradable Film, Glycerol, Potato starch, thermal stability.

## I. Introduction

In recent years, thermoplastic packaging has grown considerably. They rank first among packaging materials (58%). These materials have the advantage of being inexpensive (raw material), lighter, impact resistant and easy to process (processing temperatures below 300°C) [1].

Around 348 million tons of plastics were produced in 2018 worldwide, and their production and consumption continue to increase. The waste from these plastics causes serious environmental pollution. One of the strategies to solve this pollution problem is the complete recycling of waste. However, the recycling of these materials is limited and consumes a considerable amount of energy [2]. This issue has raised awareness about the need to put in place plastic materials that are more respectful of the environment, made up of renewable and short-lived raw materials known as biodegradable polymers [3].

Starch occurs in the form of semi-crystalline granules composed of two polysaccharides, amylose and amylopectin, which are responsible for the particular physicochemical, functional, and edible properties of starch. Amylopectin is the ramified component formed of glucose units linked by alpha (1-4) bonds in the linear sections and of alpha (1-6) bonds in the ramifications. Amylose is the linear component involved in starch gelatinization and retro gradation (hardness of starch-based products). Granules also contain a small amount of protein, fatty acids, and minerals that influence some physicochemical properties of this polymer [4, 5]. Many studies have been applied to produce starch-based polymer for conserving the petrochemical resources and reducing environmental impact. However, starch based bioplastic film have some drawbacks including poor mechanical properties and long term stability caused by water absorption and retrogradation. To overcome these limitations, plasticizer such as glycerol has been added to improve shelf-life and elasticity

of the product [6].

In this research, starch is prepared from potato and edible film is made from prepared starch plasticized with glycerol

## II. Materials and Methods

### II.1. Materials

In this research, the plant material selected as valuable raw material in the preparation of bioplastic film was the white potatoes (*Solanum tuberosum* L.) which were purchased from Bejaia local market. Glycerol (MW=92.09) was used as a plasticizer in the filmogenic solution to increase the flexibility and plasticity of the film. Hydrochloric acid (MW=36.46) promotes the destruction of the starch grain by a controlled hydrolysis phenomenon that separates amyloses/amylopectin so that the amylose goes into solution. Distilled water was used to make the solution of starch.

### II.2. Methods

Starch extraction was carried out according to the protocol described by Hirpara et al [7]. Figure 1 summarizes the main extraction steps.

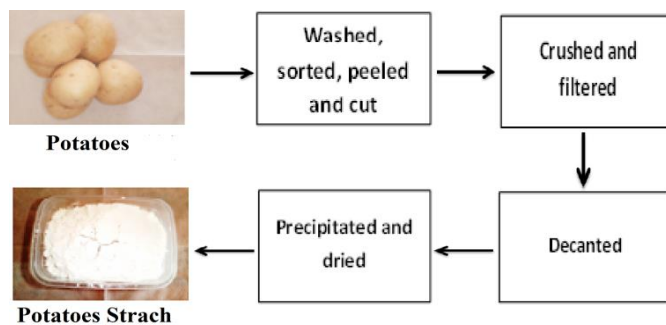


Figure 1: Main stages of starch extraction from potatoes

The films were prepared by casting technique using a film-forming solution containing potato starch 5g and Glycerol Concentration (20 and 30 %) was taken as variable parameter. 100 ml distilled water was added to it. The mixture of dry starch, water and glycerol was taken in a flask. Then 3 ml of Hydrochloric acid (0.1N) was added to the solution. The mixture was mixed with the help of glass rod on heating with stirring on magnetic stirrer at 40°C for 5 minutes. Now the mixture was kept in water bath at 85°C temperature for 15 minutes and continuously agitated by glass road. Now a cast was prepared and the entire solution was poured on the cast and was left for drying at room temp for 24 hrs. After drying the films were peeled off and were kept in polythene bags away from moisture.

### II.2.1. Moisture rate

Film moisture content was determined by drying small pieces of film in an oven at 105°C for 6 h. Knowing the mass of the film before ( $m_1$ ) and after ( $m_2$ ) stoving, the moisture content can be determined from the relation (1)

$$\text{Moisture rate (\%)} = \frac{m_0 - m_f}{m_0} \times 100 \quad (1)$$

### II.2.2. Spectroscopic characterization (FTIR)

The IRTF spectra of the different samples were recorded in absorbance mode using an infrared spectrometer model SHIMADZU FTIR-8400S, the analysis is carried out on thermoplastic films. The scanning range is between 400 and 4000  $\text{cm}^{-1}$  with a number of scans of 32 and a resolution of 4  $\text{cm}^{-1}$ .

### II.2.3. Thermal characterization

The thermograms of the different samples were recorded using a thermogravimetric device of the type (SETAREM TGA 92), controlled by a microcomputer. A mass of 10 to 20 mg is introduced into an aluminum crucible. The mass loss is measured using a thermo balance under an inert nitrogen atmosphere in a temperature range of 20 to 700°C with a heating rate of 10°C/min.

### II.2.4. Biodegradability test

The biodegradation of the samples was evaluated by measuring the mass loss of the composites as a function of time in a compost environment. Samples of size 30mm\*30mm were weighed and buried in compost boxes at a depth of 12 to 15 cm. after 2 days. The buried samples were removed, washed with distilled water then dried in an oven at 50°C for 6 hours. The samples were then weighed before returning them to the compost at 2 day intervals for a 21 day period.

The evaluation of the mass loss was calculated according to the following formula (2):

$$\text{Mass loss (\%)} = \frac{m_i - m_f}{m_i} \times 100 \quad (2)$$

With:

$m_f$ : the final mass of the sample tested.

$m_i$ : the initial mass of the sample tested.

## III. Results and Discussion

### III.1. Moisture rate

The result of moisture content of potato starch biofilm are illustrated in Table I. The maximum moisture content was observed for the combination 5 g of starch concentration and 30% glycerol this has been explained in a previous study that glycerol comprises of hydroxyl group which has an affinity for water molecules that allowing them to make hydrogen bonds and contain water in the structure. The result in agreement with the results reported in literature [8, 9].

Table 1: Moisture rate of potatoes starch biofilms

Biofilms	Moisture rate (%)
20% Glycerol	26
30% Glycerol	28

### III.2. Spectroscopic FTIR

The FT-IR spectrum curve of prepared bioplastic film was shown in Fig 2. The band at 3247  $\text{cm}^{-1}$  was represented the presence of alcohol and phenol group which has -OH stretching vibration [10]. The band at 2923  $\text{cm}^{-1}$  was indicated the alkynes group which has C-H stretching vibration [11]. The existence of C=O stretching vibration of carbonyl groups showed up the peak at 1659  $\text{cm}^{-1}$ [12]. The frequency at 1342  $\text{cm}^{-1}$  was corresponded to the presence of C-O-C stretching vibration of the aldehyde group [13]. The band at 1019  $\text{cm}^{-1}$  was also represented the characteristics of C-O stretching vibration of alcohol and phenol group. This analysis showed that the 30% and 20% glycerol films have the same chemical structure and no functional group changes occurred. FT-IR spectra exhibited that the intermolecular interaction in bioplastic occurred through C-O-H, O-H, C-H, C=O, C-O groups, it can be proved that this bioplastic was completely biodegradable [14].

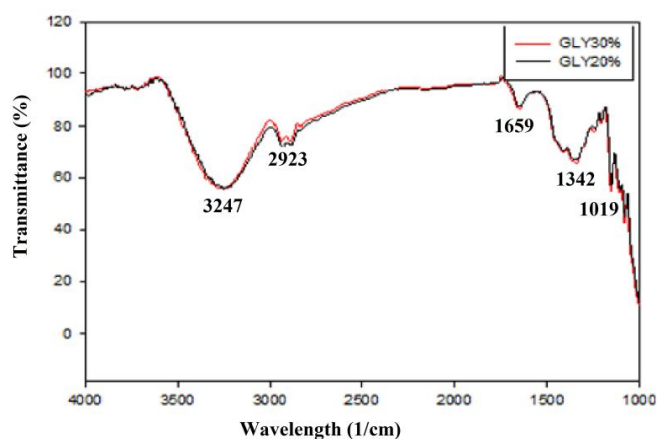


Figure 2: FT-IR Spectrum of Prepared Bioplastic film

### III.3. Thermal stability

The thermal decomposition of the two biofilms was carried out by thermogravimetric analysis (TG/DTG). From the TG thermograms of the different materials, it was possible to derive the values of the decomposition temperatures at 10, 50 % (T<sub>10%</sub> and T<sub>50%</sub>) of mass loss (Table 2). According to the results illustrated in Table 2, it was found that the film prepared with 30% of the glycerol is the most thermally stable compared to that with 20%. These results were similar to those reported in the literature [15,16]. The thermal stability of the film was increase with increased the glycerol content. This behavior could be explained because increasing the glycerol content promotes the formation of more hydrogen bridges with starch (hydrophilic nature of biopolymers and presence of voids in their structure).

Table 2: Degradation temperature of Potatoes starch biofilms

Temperature (°C)/ Biofilms	20% Glycerol	30% Glycerol
T <sub>10%</sub>	170	179
T <sub>50%</sub>	322	340

### III.4. Biodegradability test

According to the results of the biodegradable property of prepared biodegradable plastic films are shown in Figure 3, it can be seen that prepared biodegradable plastic film was completely biodegrade after 21 days of exposure to soil. It is suggested that this degradation was due two main stages of degradation: Firstly, the diffusion of the water into the film samples resulted in the swelling of the films then, allowed the growth of microorganism on the film and enzymatic and other secreted degradation caused a weight loss and disruption of the film samples [17-20].

After 21 days, complete biodegradation of the sample (GLY30%) is noticed and pores are more apparent in the sample (GLY20%), indicating a higher level of biodegradation. The rate of weight loss (GLY30%) was significantly accelerated compared to (GLY20%). The weight loss of the samples reached nearly 90% for (GLY20%) and 99% for (GLY30%). The hydroxyl groups of glycerol can form strong hydrogen bonds with the hydroxyl groups on the starch, thus, improving the interactions between the molecules, improving the cohesiveness of biopolymer matrix, and decreasing the lost mass.

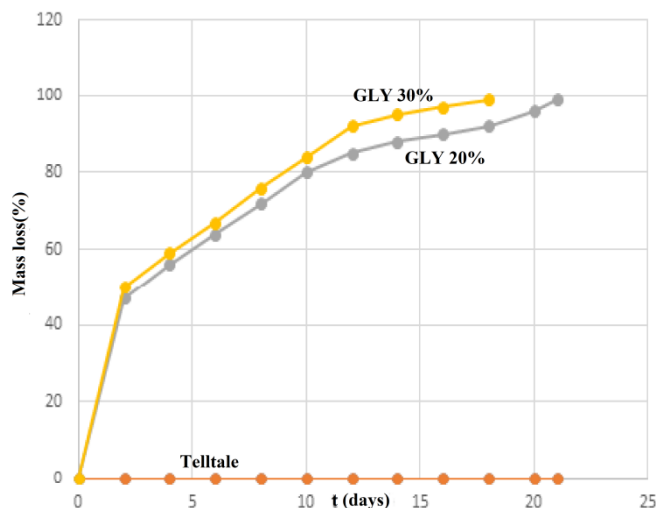


Figure 3: Biofilms mass loss rate

### IV. Conclusions

The objective of this work is to develop and characterize biodegradable biofilms based on starch, plasticized by glycerol (20 and 30%). The elaboration of the biofilms was carried out by the casting method under simple conditions. The samples were characterized by infrared spectroscopy analysis with Fourier transform (FTIR), thermogravimetric analysis and biodegradability test. Infrared spectral analysis showed that the 30% and 20% glycerol films have the same chemical structure and no functional group changes occurred. Thermogravimetric analysis showed that a 30% glycerol film has higher thermal stability than a 20% glycerol film. Biodegradability test showed that the lower the percentage of glycerol, the more easily the biofilm degrades.

**Disclosure of interest:** The authors report no conflict of interest.

### References

- [1] N. Gontard, V. Guillard, S. Gaucel, and C. Guillaume. L'emballage alimentaire et l'innovation écologique dans toutes leurs dimensions. *Journal of Innovation Agronomic*, 58, 1-9, 2017.
- [2] H. Niu, M. Zhang, X. Xia, Q. Liu, and B. Kong. Effect of porcine plasma protein hydrolysates on long-term retrogradation of corn starch. *Food Chemistry*, 239, 172–179, 2018.
- [3] L. Klaai, D. Hammiche, A. Boukerrou and V. Pandit. Thermal and Structural Analyses of Extracted Cellulose from Olive Husk. *Journal Materiel Today's*, 52, 104–107, 2022.
- [4] F. Matta Fakhouri, G. F. Nogueira, R. A. de Oliveira, and J. I. Velasco. Bioactive edible films based on arrowroot starch incorporated with cranberry powder: microstructure, thermal properties, ascorbic acid content and sensory analysis. *Polymers*, 11(10), 1650, 2019.
- [5] R. Hussain, H. Vatankhah, A. Singh, and H. S. Ramaswamy. Effect of high-pressure treatment on the structural and rheological properties of resistant corn

- starch/locust bean gum mixtures. *Journal of Carbohydrates Polymer*, 150, 299–307, 2016.
- [6] A. N. Frone, C. A. Nicolae, R. A. Gabor, and D. M. Panaitescu. Thermal properties of water-resistant starch – polyvinyl alcohol fitlatin/potato starch edible biocomposite films: Correlation between morphology and physical properties, *Journal of Carbohydrates Polymer*, 157, 1162–1172, 2017.
- [7] N.J. Hirpara, N.J.Dabhi, and P.J. Rathod. Development of Potato Starch Based Biodegradable Packaging Film. *Journal Biological Forum*, 13, 529-541, 2021.
- [8] P. Pająk, I. Przetaczek-Rożnowska, and L. Juszczak, Development and physicochemical, thermal and mechanical properties of edible films based on pumpkin, lentil and quinoa starches. *Journal of Biological Macromolecules*, 138, 441–449, 2019.
- [9] H. Zhang, F. Xu, Y. Wu, H.-H. Hu, and X.-F. Dai. Progress of potato staple food research and industry development in China. *Journal of Integrative Agriculture*, 16, 2924–2932, 2017.
- [10] M. L. Sanyang, S. M. Sapuan, M. Jawaid, M. R. Ishak, and J. Sahari. Effect of plasticizer type and concentration on physical properties of biodegradable films based on sugar palm (arenga pinnata) starch for food packaging. *Journal of Food Science Techologie*, 53, 326–336, 2015.
- [11] S. M. A. Razavi, A. M. Amini, and Y. Zahedi, Characterisation of a new biodegradable edible film based on sage seed gum: Influence of plasticiser type and concentration, *Food Hydrocolloids*, 43, 290–298, 2015.
- [12] H. Li, F. Zhai, J. Li. Physicochemical properties and structure of modified potato starch granules and their complex with tea polyphenols. *International Journal of Biological Macromolecules*, 166, 521–538, 2020.
- [13] R. -akur, P. Pristijono, C. J. Scarlett, M. Bowyer, S. P. Singh, and Q. V. Vuong. Starch-based films: major factors affecting their properties. *Journal of Biological Macromolecules*, 132, 1079–1089, 2019.
- S. Seyedi, A. Koocheki, M. Mohebbi, and Y. Zahedi. *Lepidium perfoliatum* seed gum: A new source of carbohydrate to make a biodegradable film. *Carbohydrates Polymers*, 101, 349–358, 2014.
- [14] J. Glusac, I. Davidesko-Vardi, S. Isaschar-Ovdat, B. Kukavica, and A. Fishman. Gel-like emulsions stabilized by tyrosinasecrosslinked potato and zein proteins. *Food Hydrocolloids*, 82, 53–63, 2018.
- [15] J. Glusac, I. Davidesko-Vardi, S. Isaschar-Ovdat, B. Kukavica, and A. Fishman, Gel-like emulsions stabilized by tyrosinasecrosslinked potato and zein proteins, *Food Hydrocolloids*, 82, 53–63, 2018.
- [16] C. L. Luchese, T. Garrido, J. C. Spada, I. C. Tessaro, and K. de la Caba. Development and characterization of cassava starch films incorporated with blueberry pomace, *Journal of Biological macromolecules*, 106, 834–839, 2018.
- [17] A. Haddarah, A. Bassal, A. Ismail. Structural characteristics and rheological properties of Lebanese locust bean gum. *Journal Food Engineering*, 120, 204–214, 2014.
- [18] X. Zhai, J. Shi, X. Zou. Novel colorimetric films based on starch/polyvinyl alcohol incorporated with roselle anthocyanins for fish freshness monitoring. *Food Hydrocolloids*, 69, 308–317, 2017.
- [19] J. Sahari, S. Sapuan, E. Zainudin, and M. Maleque, Physico-chemical and Thermal Properties of Starch Derived from Sugar Palm Tree (*Arenga pinnata*), *Asian Journal of Chemistry*, 26, 955–959, 2014.
- [20] J. Sahari, S. Sapuan, E. Zainudin, and M. Maleque, “Physico-chemical and Thermal Properties of Starch Derived from Sugar Palm Tree (*Arenga pinnata*), *Asian Journal of Chemistry*, 26, 955–959, 2014.

# Evaluation of mechanical and water absorption properties of polypropylene/recycled poly(ethylene terephthalate) blends

Badrina DAIRI<sup>1,2\*</sup>, Nadira BELLILI<sup>1,2</sup>, Hocine DJIDJELLI<sup>2</sup>, Amar BOUKERROU<sup>2</sup>

<sup>1</sup> Department of Process Engineering, Faculty of Technology, Skikda University 20 August–1955 – Algeria

<sup>2</sup> Department of Process Engineering, Faculty of Technology, Laboratory of Advanced Polymer Materials (LMPA), Abderrahmane MIRA University, Béjaïa 06000, Algeria

Corresponding author\*: [b.dairi@univ-skikda.dz](mailto:b.dairi@univ-skikda.dz); [badrina\\_d@yahoo.fr](mailto:badrina_d@yahoo.fr)

Received: 12 May 2022; Accepted: 12 June; Published: 21 July 2022

## Abstract

*This study is part of the recovery and mechanical recycling of polyethylene terephthalate (PET) waste, which is an abundant deposit due to its use in the packaging sector. Mixtures were prepared by melting, the effect of the composition of r-PET and MAPP was followed by morphological and mechanical studies. The results were discussed in relation to base polymers. In the absence of the compatibilizing agent (MAPP), PP/r-PET mixtures at different concentrations of r-PET exhibit a clear phase separation with poor dispersion of r-PET in the PP matrix. The addition of MAPP in PP/r-PET mixtures results in a decrease in the particle size of the dispersed phase (r-PET) in the PP matrix and an improvement in the interfacial conditions. This results in an improvement of the mechanical properties at traction and bending.*

**Keywords** Polyethylene terephthalate, compatibilizing agent, Polymer blend, Polypropylene, mechanical properties.

## I. Introduction

A recent notion (which is increasingly taken into account in our daily lives) is the notion of sustainable development, depending in part on the reduction of waste and/or its management. This goes through their treatment with a view to their recovery or recycling. A large part of the waste is made up of plastic materials used in convenience products, household appliances, construction, transport, etc.

Unfortunately, plastics, in general, have a major drawback which is their resistance to biodegradation. One of the possible solutions to reduce or eliminate them is recycling. This may be mechanical or chemical.

Mechanical recycling involves reusing the waste to make a finished or semi-finished material. However, this type of recycling generally results in a reduction in the properties of the polymer. Among these plastics, poly(ethylene terephthalate) (PET) is considered one of the most important technical polymers. PET is mainly used in the manufacture of films, fibers and containers (bottles).

PET has very good characteristics for its use in packaging: high transparency in blown containers, good mechanical properties for a minimum thickness, dimensional stability during handling (even at high temperatures), relatively low cost (price per container) and low permeability to gases such as CO<sub>2</sub> [1]. For all these reasons, PET is increasingly used as packaging material. Its widespread use generates large quantities of waste which require the implementation of recycling techniques.

Recycling PET is not easy because of its degradation during reprocessing caused by temperature, humidity and contaminants. The degradation leads to a decrease in molecular weight and loss of properties [2]. One way to improve the properties of recycled polymers is to mix them

with unmodified polymers (polyolefins) with good properties. Polypropylene (PP) is widely used in this case [3], due to its good properties (lightness, transparency, high mechanical resistance, electrical insulation, inertia to chemical aggression and use at high temperatures) [4]. It has been reported that blends of polyolefins (especially polyethylene (PE) and PP) and PET can exhibit good mechanical characteristics and permeability.

However, PET and polyolefins have very different chemical structures, which makes them immiscible with each other. The major disadvantage resulting from this incompatibility is that the resulting mixtures have poor mechanical properties.

The most frequently used means of partially filling this performance gap is compatibilization, which consists in creating chemical affinities between the constituents of the mixture in order to reduce interfacial tensions, improve adhesion between the phases and stabilize the morphology [5].

Some of these studies have focused on techniques to improve compatibility between the two polymers [6,7]. Maleic anhydride grafted MAPP may be used as a compatibilizing agent in PP/PET-r mixtures [8, 9, 10]. It has been reported that the use of MAPP in PP/PET-r mixtures can improve dispersion and adhesion between the two components [8]. It has also been indicated that the use of MAPP as a compatibilizing agent improves the strength and rigidity of PP/PET-r polymer mixtures [9]. Therefore, the main objective of this study was to investigate MAPP effect on the morphology and physico-mechanical properties of PP/r-PET blends.

## II. Material and methods

PP 500P polypropylene with a melt flow index of 3.00 g/10min was provided by SABIC Basic Industries Corporation

(Saudi Arabia). Poly(ethylene-terephthalate) (r-PET), or waste r-PET, was recovered from waste mineral water bottles. The size of r-PET pieces ranged from 2 to 5 mm. Maleic anhydride-grafted-polypropylene (MAPP) with a melt flow index of 2.63 g/10 min was provided by Arkema (Insa de Lyon, France).

### II.1. Blend preparation

Several formulations based on a PP/PET-r mixture were prepared, in the presence and in the absence of the compatibilizing agent MAPP according to the compositions indicated in Table PET-r flakes were dried at 120 °C for 24 h to remove any trace of water that may cause hydrolytic degradation of the material during use. The PP/r-PET blend (matrix) was extruded at the melting temperature of PET at 265°C and 120 rpm for 2 min using a laboratory scale co-rotating twin-screw mini extruder (15mL Micro compounder, DSM Xplore, University A. Mira of Bejaia, Algeria). The compounds were subsequently injection molded using a laboratory scale injection-molding machine (12mL Micro injection Molder, DSM Xplore, University A. Mira of Bejaia, Algeria) at 180°C barrel temperature, 90°C mold temperature, and 10 bars injection and holding pressure. Samples were molded for mechanical and physical characterization.

Table 1. Formulations of PP/r-PET blend

Sample	Table Column Head		
	PP (wt%)	r-PE T (wt %)	MA-g-PP (wt%)
PP/r-PET <sub>10</sub>			
PP/r-PET <sub>10</sub> /2,5%MA-g-PP	90	10	0
PP/r-PET <sub>10</sub> /5%MA-g-PP	87,5	10	2,5
PP/r-PET <sub>10</sub> /10%MA-g-PP	85	10	5
PP/r-PET <sub>20</sub>	80	10	10
PP/r-PET <sub>20</sub> /2,5%MA-g-PP	80	20	0
PP/r-PET <sub>20</sub> /5%MA-g-PP	77,5	20	2,5
PP/r-PET <sub>20</sub> /10%MA-g-PP	75	20	5
PP/r-PET <sub>30</sub>	70	20	10
PP/r-PET <sub>30</sub> /2,5%MA-g-PP	10	30	0
PP/r-PET <sub>30</sub> /5%MA-g-PP	67,5	30	2,5
PP/r-PET <sub>30</sub> /10%MA-g-PP	65	30	5
PP/r-PET <sub>30</sub> /10%MA-g-PP	60	30	10

### II.2. Characterizations

Sample morphology was performed on Hitachi S- 3500N Variable Pressure Scanning Electron Microscope (Hitachi High Technologies Canada) with an accelerating voltage of 20.0 kV. Specimens were freeze-fractured in liquid nitrogen and then coated with a thin layer of carbon for characterization.

Tensile and flexural tests were conducted with a Universal Testing Machine (Zwick/Roell Z020) at a crosshead speed of 5mm/min and 1.1 mm/min at room temperature according to ASTM D-638 and D-790, respectively. Five samples of each type were tested and average values were reported.

Water absorption of the PP/r-PET blends with and without MAPP was determined according to ASTM D570. Samples were immersed in distilled water at 23°C. The percentage of water absorption was calculated with the following equation (1):

$$WA = \frac{w-w_0}{w_0} \times 100 \quad (1)$$

### III. Results and discussion

#### III.1. Morphology of Blends

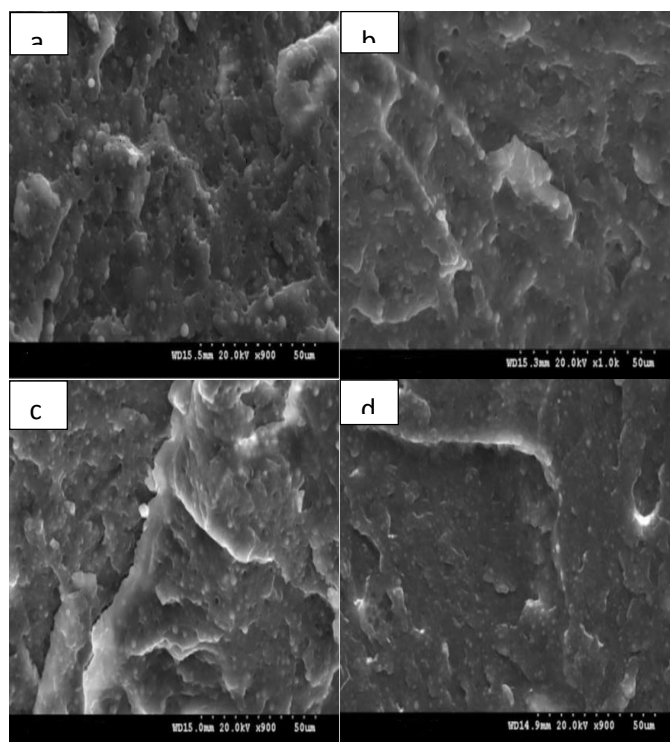


Figure 1: SEM micrograph of PP / r-PET 80/20 blend (a), SEM micrograph of the blend of PP / r-PET / 2.5% MAPP (b), SEM micrograph of the blend of PP/r-PET/ 5% MAPP, SEM micrograph of the blend of PP/r-PET /10% MAPP.

Analysis of the surface morphology of the three samples, shows the presence of a homogeneous surface characterized by a reduction in the size of the particles of r-PET embedded in the PP matrix in comparison with the non-compatible PP/r-PET mixture micrograph (Figure 10.a). This reduction in the size of the dispersed phase is significant with the increase in the content of MAPP. The morphology change is the result of



interfacial interactions between the r-PET particles and the PP matrix. The addition of 10% MAPP significantly reduces the size of r-PET particles: the PET-r particle size is changed from 2,88  $\mu\text{m}$  for the non-compatible PP/r-PET20 mixture to 2,02  $\mu\text{m}$ , 1,75 and 0,77  $\mu\text{m}$  for PP/r-PET 20 /2,5% MAPP mixtures, PP/r-PET/5% MAPP and PP/r-PET/10% MAPP, respectively.

In addition, the PET-r particles appear to be "included" in the PP matrix, this can be explained by the chemical bonds created between PET-r and PP-g-MA, thus forming anchor points between phases, and on the other hand, the absence of voids as well as the homogeneity of the structure, which suggests the existence of a certain cohesion between the matrix and the dispersed phase.

### III.2. Mechanical Properties

The presence of MAPP in PP/r-PET mixtures (Figure 5) increases elongation at break compared with completely incompatible PP/r-PET binary blends. This increase is more significant with the increase in the rate of MAPP. This indicates improved interfacial adhesion between the two components. Consequently, the blends can withstand tensile deformation at higher elongations.

PP/r-PET/MAPP ternary blends are relatively less rigid than PP/r-PET binary blends. Indeed, MAPP, due to its compatibilizing role, improving the interfacial interactions between r-PET and PP, also provides flexibility to the PP / r-PET blend. indicates improved interfacial adhesion between the two components. Consequently, the blends can withstand tensile deformation at higher elongations.

PP/r-PET/MAPP ternary blends are relatively less rigid than PP/r-PET binary blends. Indeed, MAPP, due to its compatibilizing role, improving the interfacial interactions between r-PET and PP, also provides flexibility to the PP / r-PET blend.

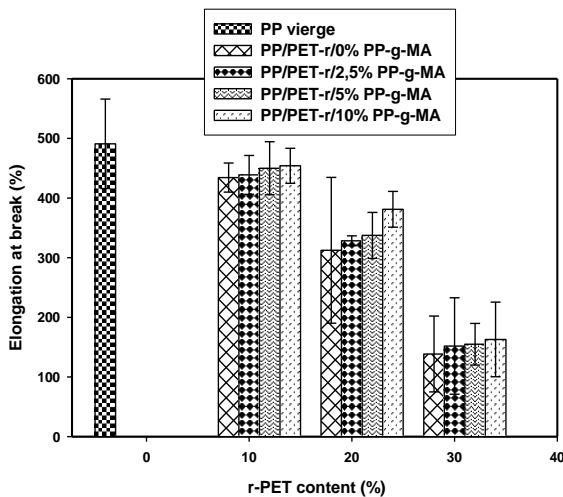


Figure. 2: Evolution of the elongation at break of PP/r-PET mixtures as a function of the rate of r-PET, in the presence of MA-g-PP.

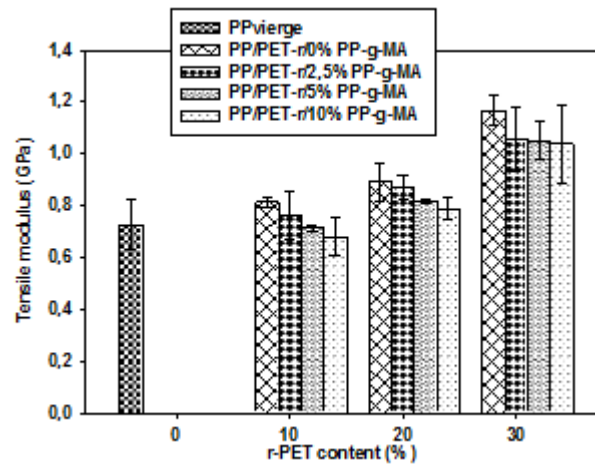


Figure. 3: Evolution of the Young's modulus of PP / r-PET blends as a function of the rate of r-PET, in the presence of MA-g-PP.

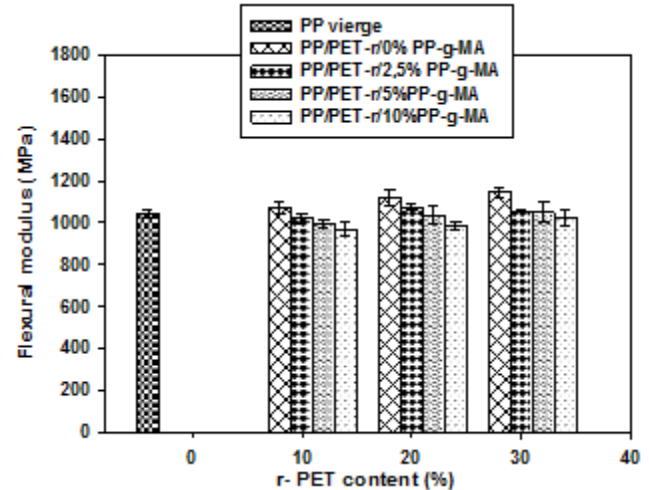


Figure. 4: Evolution of the flexural modulus of PP/r-PET blends as a function of the rate of r-PET, in the presence of MAPP.

In the presence of the MAPP copolymer, the behavior of PP/PET-r mixtures is reversed, where the modulus of traction and flexion decreases in the same range of composition which is due to an elastomeric behavior of this copolymer [11].

The transition from the brittle behavior of the PP/r-PET mixture to the ductile behavior for PP/r-PET/MAPP mixtures could be attributed to the more uniform morphology of the latter and by better adhesion in ternary mixtures compared with the PP/r-PET binary mixtures [11]. These results confirm the effectiveness of MAPP as a compatibilizer for PP / r-PET blends, causing a decrease in Young's modulus and flexural modulus.

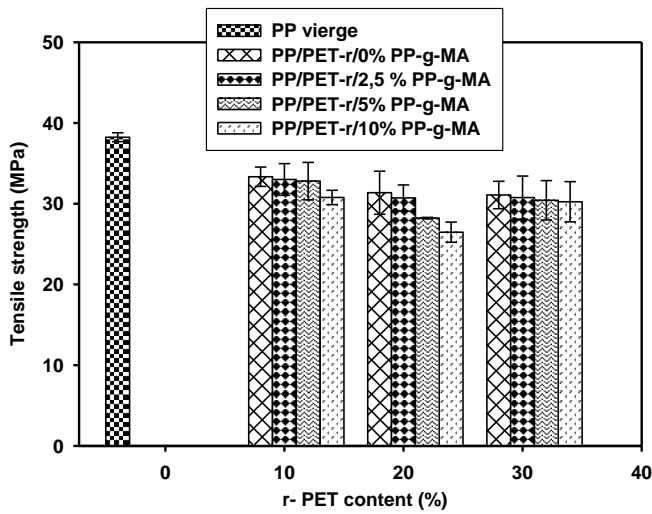


Figure 5: Evolution of the tensile stress of PP / r-PET blends as a function of the rate of r-PET, in the presence of MAPP.

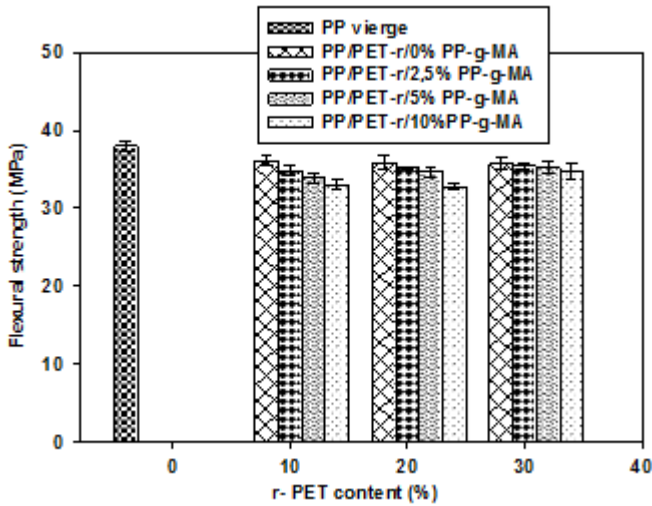


Figure 6: Evolution of the flexural stress of PP / r-PET blends as a function of the rate of r-PET, in the presence of MAPP.

We observe that the general trend of the histograms is similar for all the mixtures with different levels of r-PET, characterized by a slight decrease in tensile and flexural stress with the increase in the content of MAPP. This decrease is attributed to the elastomeric behavior of MAPP [12].

### III. 3. Fourier Transforms Infrared Spectroscopy Measurements (FTIR)

Examination of the interface between the PP and the PET-r allows for further information on the effect of compatibility on polymer blends. At the same time, the analysis of the infrared spectra of the mixtures will make it possible to establish the link between the interface and the compatibilization reaction.

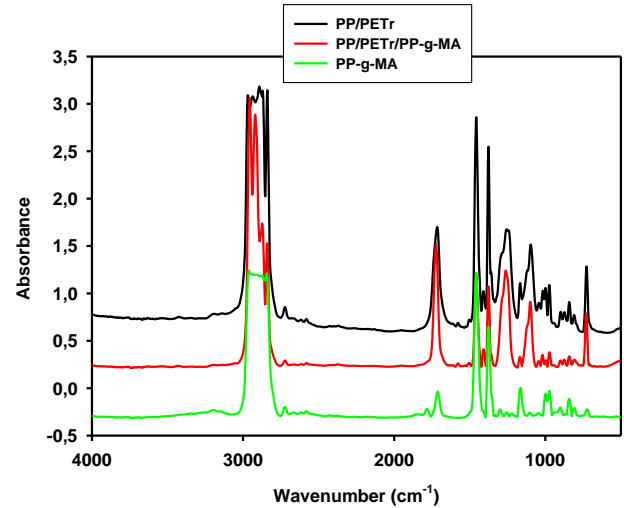


Figure 7: Infra-red spectra of PP / r-PET (80/20) blend, in the absence and in the presence of MAPP.

The spectroscopic study of the mixture to establish the chemical reaction of functional groups of MAPP with end groups of r-PET. Analysis of infrared spectra of PP / r-PET<sub>20</sub> (80/20) blend compatibilized by 10% MAPP (Figure 7) does not show a peak at 1784 cm<sup>-1</sup>, characteristic of the maleic anhydride function. This means that all of the maleic anhydride functions were indeed consumed during the reaction of compatibility with the r-PET hydroxyl groups [13].

### III. 4. Water absorption properties

It can be clearly seen from the experimental curves (Fig 8,9,10,11) that the water absorption rate of r-PET is higher than that of PP due to the hydrophilic group (ester groups) of r-PET.

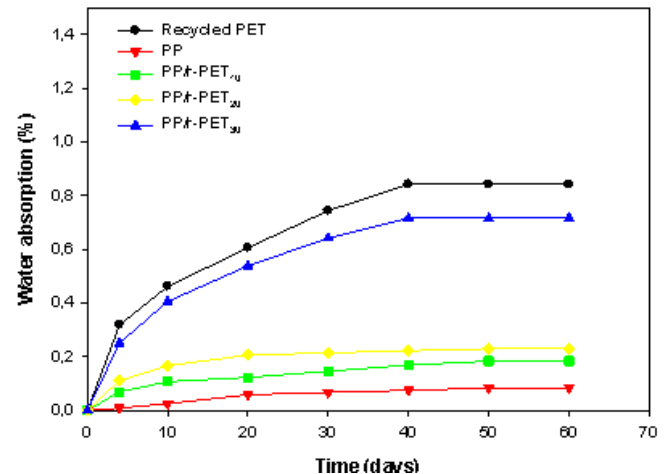


Figure 8: Evolution of the water absorption rate of PP/r-PET blends as a function of the immersion time at different rate of r-PET, in the absence of MAPP.

The increase in PET-r results in an increase in water absorption. This increase is attributed to the increase in the concentration of ester groups that have a high affinity with water. We can also attribute this phenomenon to the poor interfacial adhesion between the two phases resulting in the increase of microvoids [14]. For example, samples of PP/PET-

$r_{10}$  and PP/PET- $r_{20}$  blends reached their water saturations (0.18%, 0.23% respectively) after 30 days of immersion. However, the sample PP/PET- $r_{30}$  reached a maximum absorption (0,7 %) after 60 days of immersion compared to PP/PET- $r_{10}$  and PP/PET- $r_{20}$ .

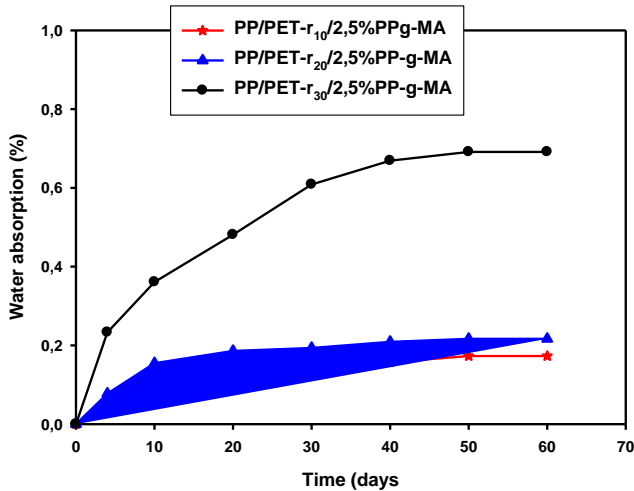


Figure. 9: Evolution of the water absorption rate of PP/r-PET blends as a function of the r-PET rate, in the presence of 2.5% MA-g-PP.

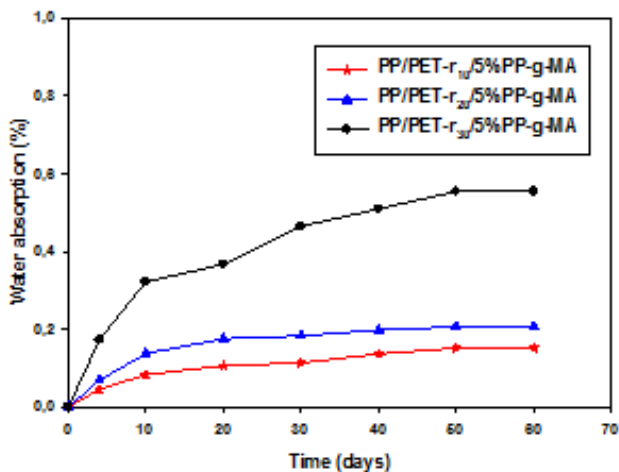


Figure. 10: Evolution of the water absorption rate of PP/r-PET mixtures as a function of the r-PET level, in the presence of 5% MA-g-PP.

The introduction of MAPP into PP/r-PET blends at different levels of r-PET reveals reduced water absorption compared to non-compatible PP/r-PET blends (Figure 1), this reduction is more significant with the increase in the rate of MAPP, this is attributed to an improvement in the interfacial adhesion between the dispersed phase and the polymer matrix and consequently a considerable decrease in the microvoids which promote water absorption [15].

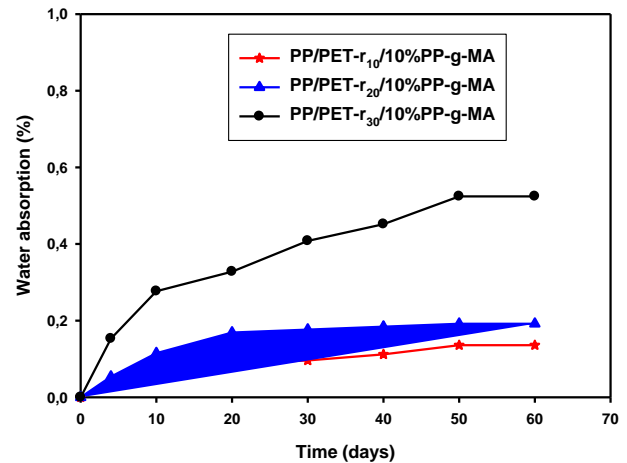


Figure. 11: Evolution of the water absorption rate of PP/r-PET blends as a function of the r-PET rate, in the presence of 10% MA-g-PP.

#### IV. Conclusions

During this study devoted to the study of the optimization of the rate of the compatibilizing agent PP-g-MA, we have been particularly interested in the problem of the PP/PET-r interface at different PP-g-MA rates, by varying the rate of 2.5, 5 and 10%. The demonstration of compatibility was examined by the various analytical techniques.

All the results obtained indicate that the addition of PP-g-MA as a compatibilizing agent improves the morphology of the PP/PET-r polymer blends at different rate of MAPP. These results in a reduction in the size of the particles of PET-r embedded in the PP matrix and an improvement in the interfacial adhesion between the two polymers. In addition, a decrease in Young's modulus and flexural modulus is also observed with an increase in elongation at break. The infrared spectra confirm that the reaction between the hydroxyl groups of PET-r and the maleic anhydride functions of MAPP has occurred giving a PP-g-PET copolymer. The introduction of MAPP into PP / PET-r blends at different rate of PET-r reveals reduced water absorption compared to non-compatible PP/PET-r blends. This is attributed to an improvement in the interfacial adhesion between the dispersed phase and the polymer matrix.

**Disclosure of interest:** The authors report no conflict of interest.

#### References

- [1] I. Tan, Ahmad, M. Heng. Characterization of polyester composites from recycled polyethylene terephthalate reinforced with empty fruit bunch fibers, *Materials and Design*, 32, 4493-4501, 2011.
- [2] N.G. Karsli, S. Yesil, A. Aytac, Effect of short fiber reinforcement on the properties of recycled poly (ethylene terephthalate)/poly(ethylene naphthalate) blends, *Materials and Design*, 46, 867-872, 2013.
- [3] Y.X. Pang, D.M. Jia, H.J. Hu, D.J. Hourston, M. Song, Effects of a compatibilizing agent on the morphology,

- interface and mechanical behaviour of polypropylene/poly(ethylene terephthalate) blends, *Polymer*, 41, 357-365, 2000.
- [4] M. Kaci, A. Hamma, I. Pillin, Y. Grohens. Effect of Reprocessing Cycles on the Morphology and Properties of Poly(propylene)/Wood Flour Composites Compatibilized with EBAGMA Terpolymer, *Macromolecular Materials and Engineering*, 294, 532-540, 2009.
- [5] P. Van Puyvelde, S. Velankar, P. Moldenaers, Rheology and morphology of compatibilized polymer blends, *Current Opinion in Colloid and Interface Science*, 6, 457-463, 2001.
- [6] M.F. Champagne, M. A. Huneault, C. Roux, W. Peyrel, Reactive compatibilization of polyethylene terephthalate/polypropylene blends, *Polymer Engineering and Science*, 39, 976-984, 1999.
- [7] C.P. Papadopoulou, N.K. Kalfoglou, Comparison of compatibilizer effectiveness for PET/PP blends: their mechanical, thermal and morphology characterization, *Polymer*, 41, 2543-2555, 2000.
- [8] K.H. Yoon, H.W. Lee, O.O. Park, Properties of poly(ethyleneterephthalate) and maleic anhydride-grafted polypropylene blends by reactive processing, *Journal of Applied Polymer Science*, 70, 389-395, 1998.
- [9] M.K. Cheung, D. Chen, Mechanical and rheological properties of poly(ethylene terephthalate)/polypropylene blends, *Polymer International*, 43, 281-287, 1997.
- [10] M. Xanthos, M.W. Young, J.A. Biesenberger, «Polypropylene/polyethylene terephthalate blends compatibilized through functionalization, *Polymer Engineering and Science*, 30, 355-365, 1990.
- [11] T.L. Dimitrova, F.P. La Mantia, F. Pilati, M. Toselli, A. Valenza, A. Visco, On the compatibilization of PET/HDPE blends through a new class of copolyesters, *Polymer*, 41 4817-4824, 2000.
- [12] H. Zhang, W. Guo, Y. Yu, B. Li, C. Wu, «Structure and properties of compatibilized recycled poly(ethylene terephthalate)/linear low density polyethylene blends, *European Polymer Journal*, 43, 3662-3670, 2007.
- [13] Y. Tao, K. Mai, Non-isothermal crystallization and melting behavior of compatibilized polypropylene/recycled poly (ethylene terephthalate) blends», *European Polymer Journal*, 43 3538-3549, 2007.
- [14] I. Merdas, F. ThomINETTE, A. Tcharkntchi, J. Verdu, Factors governing water absorption by composite matrices, *Composites Science and Technology*, 62, 487-492, 2000.
- [15] A. Arbelaiz, B. Fernandez, J.A. Ramos, A. Retegi, R. Liano-Ponte, I. Mondragon. Mechanical properties of short flax fiber bundle/polypropylene composites: Influence of matrix/fiber modification, fiber content, water uptake and recycling, *Composites Science and Technology*, 65, 1582-1592, 2005.